

Excitonic Theory of the Ultrafast Optical Response of 2D-Quantum-Confined Semiconductors at Elevated Densities

Henry Mittenzwey,^{1,*} Oliver Voigt,¹ and Andreas Knorr¹

¹*Nichtlineare Optik und Quantenelektronik, Institut für Physik und Astronomie (IFPA),
Technische Universität Berlin, D-10623 Berlin, Germany*

(Dated: December 4, 2025)

An excitonic approach to the ultrafast optical response of confined semiconductors at elevated densities below the Mott transition is presented. The theory is valid from the coherent regime, where coherent excitonic transitions and biexcitons dominate, to the incoherent regime, where excitonic occupations dominate. Numerical simulations of the 1s exciton dynamics during intense circularly polarized pump pulses in two different Coulomb-interaction regimes are performed for two-dimensional semiconductors: Moderate Coulomb interaction is compared with dominating Coulomb interaction with respect to the light-matter interaction strength. The different many-body contributions are disentangled and it is found, that excitonic Rabi oscillations in the Coulomb-dominated regime are considerably less strong. By also comparing circular and linear excitation in a MoSe₂ monolayer, it is found, that linear excitation creates a regime, where excitonic Rabi oscillations are almost completely suppressed.

I. INTRODUCTION

Rabi oscillations [1], while first having been observed in atomic two-level systems [2], later in quantum dots [3, 4] or assisted by optical cavities [5], also occur in confined semiconductors such as quantum wells without an optical cavity [6–10]. In these structures, however, Rabi oscillations are not only determined by the usual Pauli blocking but also by Coulomb interactions between optically excited electrons and holes. Rabi oscillations in quantum wells have been successfully predicted by the semiconductor Bloch equations in Hartree-Fock limit (SBE) and observed in experiments [6, 11, 12]. However, if – in materials exhibiting strong electron-hole interactions – higher correlations beyond the Hartree-Fock limit and incoherent interaction with the phonon bath need to be taken into account, the numerical effort of the SBEs quickly increases [13]. Also, the Hartree-Fock-limit lacks any possibility to resolve correlated exciton-exciton effects [14–19] or an accurate description of intraband processes [20–22]. Therefore, for material parameters, where Coulomb interaction dominates over the light-matter interaction, such as atomically thin transition metal dichalcogenide monolayers, an excitonic theory, i.e., a formulation in electron-hole pair operators [23–25], is better suited.

In the past, several excitonic theories valid in the regime of elevated densities have been proposed: By using a momentum-independent formulation using the Usui transformation [26–29], by using a localized Wannier basis [30], by employing a strict coherent limit [17, 18, 31, 32] or via a bosonic non-equilibrium Green's function method focusing on the dynamics of optically inactive excitons via nonlinear light-matter interaction [33]. Other approaches regarding exciton dynamics in optical cavities introduce additional Hamiltonians to account for

fermionic Pauli-blocking in an otherwise bosonic excitonic description [34–36] or stay in a strict coherent limit [37–39].

Hence, a comprehensive and microscopic momentum-resolved theory for Wannier-Mott excitons [40] developing a consistent description of simultaneous Coulomb, light-matter and exciton-phonon interaction in an undoped quantum-confined semiconductor, which is able to bridge the gap between the coherent [14, 15, 17, 18, 41] and incoherent regime [42–46] in the low-density limit as well as in the elevated-density regime beyond the third-order susceptibility [45, 47–49], is still missing.

In this manuscript, we develop an excitonic approach for Wannier excitons up to fourth-order dynamics-controlled truncation (DCT) [24, 25] for up to three-exciton correlations needed to describe the optical response from the coherent to the incoherent regime at elevated exciton densities.

The manuscript is organized as follows: In Sec. II, we lay out the Hamiltonians of the considered interaction mechanisms. In Sec. III, we develop the exciton Bloch equations and discuss all contributions up to fourth order DCT. In Sec. IV, we study the exciton Rabi-flopping dynamics within intense pump pulses of extended duration for two different Coulomb regimes in circular excitation: A GaAs quantum well (QW) and a h-BN encapsulated MoSe₂ monolayer (ML) in circular excitation and additionally compare circular and linear excitation in a MoSe₂ ML.

II. HAMILTONIANS

The total Hamiltonian \hat{H} reads [11, 50, 51]:

$$\hat{H} = \hat{H}_0 + \hat{H}_{\text{Coul-eh}} + \hat{H}_{\text{Coul-ee}} + \hat{H}_{\text{Coul-hh}} + \hat{H}_{\text{l-m}}. \quad (1)$$

* h.mittenzwey@tu-berlin.de

\hat{H}_0 is the free Hamiltonian:

$$\hat{H}_0 = \sum_{\mathbf{k}, \xi} \left(E_{v/c, \mathbf{k}}^\xi \hat{v}_{\mathbf{k}}^{\dagger \xi} \hat{v}_{\mathbf{k}}^\xi + E_{c, \mathbf{k}}^\xi \hat{c}_{\mathbf{k}}^{\dagger \xi} \hat{c}_{\mathbf{k}}^\xi \right), \quad (2)$$

where $E_{v/c, \mathbf{k}}^\xi$ is the valence/conduction band dispersion in effective-mass approximation $E_{v/c, \mathbf{k}}^\xi = E_{v/c}^\xi \mp \frac{\hbar^2 \mathbf{k}^2}{2m_{h/e}^\xi}$ with valence/conduction band edge $E_{v/c}^\xi$ and hole/electron masses $m_{h/e}^\xi$ at momentum \mathbf{k} and spin-valley index ξ . $v^{(\dagger)}/c^{(\dagger)}$ are the valence/conduction band annihilation (creation) operators. The Coulomb Hamiltonian [51] consists of an electron-hole contribution $\hat{H}_{\text{Coul-eh}}$:

$$\hat{H}_{\text{Coul-eh}} = \sum_{\mathbf{k}, \mathbf{k}', \mathbf{q}, \xi, \xi'} V_{\mathbf{q}} \hat{v}_{\mathbf{k}+\mathbf{q}}^{\dagger \xi} \hat{c}_{\mathbf{k}'-\mathbf{q}}^{\dagger \xi'} \hat{c}_{\mathbf{k}'}^{\xi'} \hat{v}_{\mathbf{k}}^\xi, \quad (3)$$

an electron-electron contribution $\hat{H}_{\text{Coul-ee}}$:

$$\hat{H}_{\text{Coul-ee}} = \frac{1}{2} \sum_{\mathbf{k}, \mathbf{k}', \mathbf{q}, \xi, \xi'} V_{\mathbf{q}} \hat{c}_{\mathbf{k}+\mathbf{q}}^{\dagger \xi} \hat{c}_{\mathbf{k}'-\mathbf{q}}^{\dagger \xi'} \hat{c}_{\mathbf{k}'}^{\xi'} \hat{c}_{\mathbf{k}}^\xi, \quad (4)$$

and a hole-hole contribution $\hat{H}_{\text{Coul-hh}}$:

$$\hat{H}_{\text{Coul-hh}} = \frac{1}{2} \sum_{\mathbf{k}, \mathbf{k}', \mathbf{q}, \xi, \xi'} V_{\mathbf{q}} \hat{v}_{\mathbf{k}+\mathbf{q}}^{\dagger \xi} \hat{v}_{\mathbf{k}'-\mathbf{q}}^{\dagger \xi'} \hat{v}_{\mathbf{k}'}^{\xi'} \hat{v}_{\mathbf{k}}^\xi. \quad (5)$$

Here, $V_{\mathbf{q}} = \frac{e^2}{\mathcal{A}} \int dz dz' |\xi(z)|^2 G_{\mathbf{q}}(z, z') |\xi(z')|^2$ is the screened quantum-confined Coulomb potential, where e is the elementary charge, \mathcal{A} is the sample area, $\xi(z)$ is the confinement wave function and $G_{\mathbf{q}}(z, z')$ is the Green's function solving the generalized Poisson equation of the corresponding sample geometry including the dielectric environment, cf. Eq. (S68) in the Supplementary Material (SM). Coulomb exchange interaction – not to be confused with the usual contributions due to fermionic exchange – [52–54], which causes corrections to the exciton [52] or biexciton dispersion [55], intervalley scattering [56, 57] and the biexciton fine structure [16, 58], as well as Auger scattering [48, 49] and Dexter interaction [59–61], are neglected, since we focus on the most dominant (direct) Coulomb interaction processes needed to explain recent experiments [62]. However, these interaction processes can be straightforwardly included by adding the corresponding Hamiltonians.

The light-matter interaction Hamiltonian in dipole approximation reads:

$$\hat{H}_{\text{l-m}} = - \sum_{\mathbf{k}, \mathbf{Q}, \xi} \left(\mathbf{E}_{\mathbf{Q}} \cdot \mathbf{d}^{cv} \hat{c}_{\mathbf{k}+\mathbf{Q}}^{\dagger \xi} \hat{v}_{\mathbf{k}}^\xi + \text{h.a.} \right). \quad (6)$$

Here, $\mathbf{E}_{\mathbf{Q}} = \frac{1}{\mathcal{A}} \int dz |\xi(z)|^2 \mathbf{E}_{\mathbf{Q}}(z)$ is the quantum-confined optical field, where $\mathbf{E}_{\mathbf{Q}}(z)$ solves the wave equation in momentum space of the corresponding sample geometry [63] and \mathbf{d}^{cv} is the transition dipole moment in low-wavenumber approximation [64, 65]. As we excite excitonic states just below the free-particle band gap, we

neglect any intraband contributions [66]. Note, that intraband light-matter interaction can induce light-driven transport of optically excited electron-hole pairs [67], intraexcitonic transitions [68, 69] or dynamical localization [70, 71], even throughout the total Brillouin zone if the exciting pulse is strong enough [72], constituting the key ingredient for lightwave electronics [73]. However, in such a regime, the effective-mass approximation and, hence, a projection on excitonic states solving the Wannier equation, cf. Eq. (13), is not possible anymore, since we would have to take into account the full connected band structure throughout the total Brillouin zone.

III. EXCITONIC EQUATIONS OF MOTION

The excitonic equations of motion are derived as follows. We start by deriving Heisenberg's equations of motion $i\hbar \partial_t \hat{A} = [\hat{A}, \hat{H}]$ for the electron-hole pair operators \hat{A} of interest, which can contain an arbitrary but equal number of conduction/valence band annihilation (creation) operators $c^{(\dagger)}/v^{(\dagger)}$. However, after evaluating the commutator $[\hat{A}, \hat{H}]$, the appearing operator products on the right-hand side of the corresponding equation of motion do not necessarily contain an equal number of electron and hole operators. Therefore, we project all operator products, which contain an unequal number of electron and hole operators onto electron-hole pairs via the unit-operator method [23, 74]. E.g., electron and hole occupations are expanded according to (using a compound index $i = \{\mathbf{k}_i, \xi_i\}$):

$$\begin{aligned} \hat{c}_1^\dagger \hat{c}_2 &= \sum_3 \hat{c}_1^\dagger \hat{v}_3 \hat{v}_3^\dagger \hat{c}_2 - \frac{1}{2} \sum_{3,4,5} \hat{c}_1^\dagger \hat{v}_3 \hat{c}_4^\dagger \hat{v}_5 \hat{v}_5^\dagger \hat{c}_4 \hat{v}_3^\dagger \hat{c}_2 \\ &\quad + \mathcal{O}(Na_B^2)^3, \\ \hat{v}_1 \hat{v}_2^\dagger &= \sum_3 \hat{c}_3^\dagger \hat{v}_1 \hat{v}_2^\dagger \hat{c}_3 - \frac{1}{2} \sum_{3,4,5} \hat{c}_3^\dagger \hat{v}_1 \hat{c}_4^\dagger \hat{v}_5 \hat{v}_5^\dagger \hat{c}_4 \hat{v}_2^\dagger \hat{c}_3 \\ &\quad + \mathcal{O}(Na_B^2)^3. \end{aligned} \quad (7)$$

Note, that the unit-operator method corresponds exactly to the contraction theorem in Ref. [25]. Then, we evaluate the expectation values via the correlation expansion technique [75, 76]. Within this framework, the expectation values of the operator products are expanded as follows (\hat{A}_i is an arbitrary fermionic creation or annihilation operator):

$$\begin{aligned} \langle \hat{A}_1 \hat{A}_2 \rangle &= \langle \hat{A}_1 \hat{A}_2 \rangle_c \quad (\text{singlet}), \\ \langle \hat{A}_1 \hat{A}_2 \hat{A}_3 \hat{A}_4 \rangle &= \langle \hat{A}_1 \hat{A}_2 \hat{A}_3 \hat{A}_4 \rangle_c \quad (\text{doublet}) \\ &\quad + \langle \hat{A}_1 \hat{A}_2 \rangle_c \langle \hat{A}_3 \hat{A}_4 \rangle_c \\ &\quad - \langle \hat{A}_1 \hat{A}_3 \rangle_c \langle \hat{A}_2 \hat{A}_4 \rangle_c \\ &\quad + \langle \hat{A}_1 \hat{A}_4 \rangle_c \langle \hat{A}_2 \hat{A}_3 \rangle_c \\ \langle \hat{A}_1 \hat{A}_2 \hat{A}_3 \hat{A}_4 \hat{A}_5 \hat{A}_6 \rangle &= \langle \hat{A}_1 \hat{A}_2 \hat{A}_3 \hat{A}_4 \hat{A}_5 \hat{A}_6 \rangle_c \quad (\text{triplet}) \\ &\quad + \dots \end{aligned} \quad (8)$$

Here, the subscript "c" denotes the correlated part of the expectation value on the corresponding operator level, which cannot be factorized in lower contributions anymore. The sign of each term is determined by the amount of commutations necessary to disentangle the operator products. The correlated expectation values behave antisymmetric with respect to pairwise exchange:

$$\langle \dots \hat{A}_i \hat{A}_j \dots \rangle_c = -\langle \dots \hat{A}_j \hat{A}_i \dots \rangle_c. \quad (9)$$

We formulate our theory always in the truly correlated quantities $\langle \hat{A} \rangle_c$, which are obtained by subtracting all lower contributions from the total expectation value [75, 77]:

$$\langle \hat{A} \rangle_c = \langle \hat{A} \rangle - (\text{all lower correlations}). \quad (10)$$

This definition provides the clearest physical picture, since it ensures, that the corresponding quantum kinetics only include fully correlated contributions on the corresponding level (singlet, doublet, triplet etc.) and no lower-order correlations mix in. In particular, it ensures a clear separation of coherent and incoherent excitonic effects. To determine the relevant microscopic quantities, we perform a dynamics-controlled truncation (DCT) [24, 25]. This approach systematically organizes the quantum-mechanical hierarchy problem in powers of the optical field \mathbf{E} . Within the Heisenberg-equations-of-motion method, Eq. (7) provides the possibility to introduce the dynamical order m of the expectation value of an excitonic operator \hat{A}_n of order n :

$$\langle \hat{A}^{(n)} \rangle = \mathcal{O}(\mathbf{E}^m), \quad (11)$$

where $m \geq n$. Here, n is the total number of valence or conduction band creation and annihilation operators of $\hat{A}^{(n)}$. Therefore, if one wants to calculate the optical response of a semiconductor, one first has to fix the desired dynamical order m within the optical field and subsequently collects all occurring (correlated) expectation values of order $n \leq m$. To determine the order m of a specific expectation value, one counts all occurring electron-hole pairs and optical fields on the right-hand side of the corresponding Heisenberg equations of motion. After we set up all equations motion in the electron-hole picture, we perform an expansion in excitonic wave functions afterwards. This is crucial, since approaches, which apply an excitonic picture already on the Hamiltonian level are prone to miss important corrections due to the fermionic substructure of the excitons [78] within higher orders of the optical field.

We note, that the DCT-approach is similar but not equal to a strict perturbation expansion in powers of the optical field [64], which is often done for calculating, e.g., high-harmonic responses, as the DCT-approach always delivers a closed set of equations, while the strict perturbation expansion does not.

In this work, we develop the excitonic equations of motion up to fourth order, i.e., $m \leq 4$, in the optical

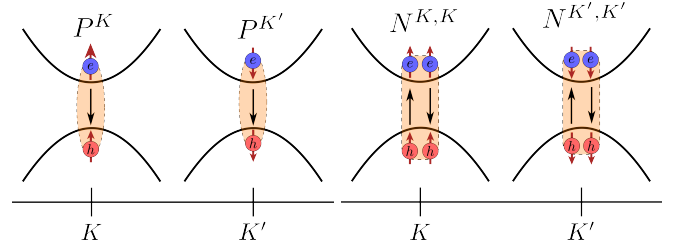


FIG. 1. Scheme of excitonic transitions in Eq. (13) at the K and K' valley (left) and excitonic occupations from Eq. (15) in intravalley configuration at the K and K' valleys (right) in a monolayer TMDC.

field up to triplets or six-particle correlations and neglect quadruplets, i.e., eight-particle correlations. In this limit, the relevant quantities are the excitonic transition P , cf. Fig. 1(left) of order $n = 1$:

$$P \sim \langle \hat{A}^{(1)} \rangle_c = \langle \hat{v}_1^\dagger \hat{c}_2 \rangle_c = \langle \hat{v}_1^\dagger \hat{c}_2 \rangle, \quad (12)$$

which in the excitonic picture explicitly reads:

$$P_\mu^\xi = \sum_{\mathbf{q}} \varphi_{\mu,\mathbf{q}}^{*\xi,\xi'} \langle \hat{v}_{\mathbf{q}}^\dagger \hat{c}_{\mathbf{q}}^\xi \rangle_c, \quad (13)$$

where $\varphi_{\mu,\mathbf{q}}^{\xi,\xi'}$ is the excitonic wave function solving the Wannier equation with excitonic quantum number μ , relative momentum \mathbf{q} , hole configuration ξ and electron configuration ξ' denoting different spins and symmetry points in the Brillouin zone, such as K, K' in atomically thin semiconductors, cf. Eq. (S1). Note, that we only consider optically excited excitonic transitions with a center-of-mass momentum of zero.

The excitonic occupations/intraexcitonic coherences ($\mu = \nu/\mu \neq \nu$) of order $n = 2$, cf. Fig. 1 (right), are defined as:

$$N \sim \langle \hat{A}^{(2)} \rangle_c = \langle \hat{c}_1^\dagger \hat{v}_2 \hat{v}_3^\dagger \hat{c}_4 \rangle_c = \langle \hat{c}_1^\dagger \hat{v}_2 \hat{v}_3^\dagger \hat{c}_4 \rangle - \langle \hat{c}_1^\dagger \hat{v}_2 \rangle \langle \hat{v}_3^\dagger \hat{c}_4 \rangle, \quad (14)$$

which in the excitonic picture explicitly read:

$$N_{\mu,\nu,\mathbf{Q}}^{\xi,\xi'} = \sum_{\mathbf{q},\mathbf{q}'} \varphi_{\mu,\mathbf{q}-\alpha_{\xi,\xi'},\mathbf{Q}}^{\xi,\xi'} \varphi_{\nu,\mathbf{q}'+\beta_{\xi,\xi'},\mathbf{Q}}^{*\xi,\xi'} \times \langle \hat{c}_{\mathbf{q}}^\dagger \hat{v}_{\mathbf{q}-\mathbf{Q}}^\xi \hat{v}_{\mathbf{q}'}^\dagger \hat{c}_{\mathbf{q}'+\mathbf{Q}}^{\xi'} \rangle_c, \quad (15)$$

where \mathbf{Q} is the center-of-mass momentum and $\alpha_{\xi,\xi'}$ and $\beta_{\xi,\xi'}$ are the effective-mass ratios of the corresponding excitonic configuration ξ, ξ' :

$$\alpha_{\xi,\xi'} = \frac{m_e^{\xi'}}{m_h^\xi + m_e^{\xi'}}, \quad \beta_{\xi,\xi'} = \frac{m_h^\xi}{m_h^\xi + m_e^{\xi'}}. \quad (16)$$

Throughout this work, we restrict the excitonic occupations/intraexcitonic coherences to carrying total momenta of $2\mathbf{Q}$, since we assume spatially homogeneous optical excitation.

As introduced by *Moskalenko* [79] and *Lampert* [80] and later explicitly calculated by *Ivanov* using a variational approach [81], the two-exciton coherence of order $n = 2$ are defined as [14, 17, 82, 83], cf. Fig. 2(left):

$$\begin{aligned} B &\sim \langle \hat{A}^{(2)} \rangle_c = \langle \hat{v}_1^\dagger \hat{c}_2 \hat{v}_3^\dagger \hat{c}_4 \rangle_c \\ &= \langle \hat{v}_1^\dagger \hat{c}_2 \hat{v}_3^\dagger \hat{c}_4 \rangle - \langle \hat{v}_1^\dagger \hat{c}_2 \rangle \langle \hat{v}_3^\dagger \hat{c}_4 \rangle + \langle \hat{v}_1^\dagger \hat{c}_4 \rangle \langle \hat{v}_3^\dagger \hat{c}_2 \rangle, \end{aligned} \quad (17)$$

which, after an exciton expansion and a consecutive biexciton expansion, explicitly read:

$$\begin{aligned} B_{\pm, \zeta}^{\xi_1, \xi_2, \xi_3, \xi_4} &= \sum_{\mu, \nu, \mathbf{Q}} \Phi_{B, \pm, \zeta, \mu, \nu, \mathbf{Q}}^{*L, \xi_1, \xi_2, \xi_3, \xi_4} \\ &\times \sum_{\rho, \eta, \mathbf{Q}'} (S_{\pm}^{-1})_{\mu, \nu, \mathbf{Q}, \rho, \eta, \mathbf{Q}'}^{\xi_1, \xi_2, \xi_3, \xi_4}(\mathbf{0}) \\ &\times \sum_{\mathbf{q}, \mathbf{q}'} \varphi_{\rho, \mathbf{q} + \beta_{\xi_1, \xi_2/\xi_4}}^{* \xi_1, \xi_2/\xi_4} \varphi_{\eta, \mathbf{q}' + \alpha_{\xi_3, \xi_2/\xi_4}}^{* \xi_3, \xi_2/\xi_4} \mathbf{Q}' \\ &\times \frac{1}{2} \left(\langle \hat{v}_1^\dagger \hat{c}_2 \hat{c}_3^\dagger \hat{v}_4^\dagger \hat{c}_4 \rangle_c \pm \langle \hat{v}_1^\dagger \hat{c}_2 \hat{c}_3^\dagger \hat{v}_4^\dagger \hat{c}_4 \rangle_c \right), \end{aligned} \quad (18)$$

where $\Phi_{B, \pm, \zeta, \mu, \nu, \mathbf{Q}}^{*L, \xi_1, \xi_2, \xi_3, \xi_4}$ is the two-exciton wave function solving the two-exciton Schrödinger equation with quantum number ζ and configuration \pm , cf. Eq. (S18). $(S_{\pm}^{-1})_{\mu, \nu, \mathbf{Q}, \rho, \eta, \mathbf{Q}'}^{\xi_1, \xi_2, \xi_3, \xi_4}(\mathbf{0})$ is the projection matrix element arising due to the expansion in symmetric (+) and antisymmetric (−) configurations with respect to electron exchange, cf. Eq. (S23). The subscript “ ξ/ξ' ” with respect to the electron configuration in the excitonic wave functions denotes an averaging over the electron configurations ξ and ξ' , if they are different, i.e., the corresponding excitonic wave functions obey the averaged Wannier equation, cf. Eq. (S1). This averaging procedure is necessary to expand the two-exciton correlations in excitonic wave functions. Throughout this work, we use the term “two-exciton coherence” to generally denote all bound and unbound two-exciton states with $\zeta = b$ or $\zeta \neq b$, while we use the term “two-exciton continuum”, if we specifically designate the continuum states with $\zeta \neq b$, and we use the term “bound biexciton”, if we specifically designate the bound two-exciton state $\zeta = b$. Note, since we only consider optically excited excitonic transitions at zero center-of-mass momentum $\mathbf{Q} = \mathbf{0}$, the two-exciton states are restricted to a total momentum of zero, which greatly reduces the relevant two-exciton phase space.

First rigorously calculated by *Axt* [24], the exciton-two-exciton transitions of order $n = 3$ are defined as, cf. Fig. 2(right) and Fig. 3:

$$\begin{aligned} Z &\sim \langle \hat{A}^{(3)} \rangle_c = \langle \hat{c}_1^\dagger \hat{v}_2 \hat{v}_3^\dagger \hat{c}_4 \hat{v}_5^\dagger \hat{c}_6 \rangle_c \\ &= \langle \hat{c}_1^\dagger \hat{v}_2 \hat{v}_3^\dagger \hat{c}_4 \hat{v}_5^\dagger \hat{c}_6 \rangle - \langle \hat{c}_1^\dagger \hat{v}_2 \rangle \langle \hat{v}_3^\dagger \hat{c}_4 \hat{v}_5^\dagger \hat{c}_6 \rangle_c \\ &\quad - \langle \hat{v}_3^\dagger \hat{c}_4 \rangle \langle \hat{c}_1^\dagger \hat{v}_2 \hat{v}_5^\dagger \hat{c}_6 \rangle_c + \langle \hat{v}_3^\dagger \hat{c}_6 \rangle \langle \hat{c}_1^\dagger \hat{v}_2 \hat{v}_5^\dagger \hat{c}_4 \rangle_c \\ &\quad + \langle \hat{v}_5^\dagger \hat{c}_4 \rangle \langle \hat{c}_1^\dagger \hat{v}_2 \hat{v}_3^\dagger \hat{c}_6 \rangle_c + \langle \hat{v}_5^\dagger \hat{c}_6 \rangle \langle \hat{c}_1^\dagger \hat{v}_2 \hat{v}_3^\dagger \hat{c}_4 \rangle_c \\ &\quad - \langle \hat{c}_1^\dagger \hat{v}_2 \rangle \langle \hat{v}_3^\dagger \hat{c}_4 \rangle \langle \hat{v}_5^\dagger \hat{c}_6 \rangle + \langle \hat{c}_1^\dagger \hat{v}_2 \rangle \langle \hat{v}_3^\dagger \hat{c}_6 \rangle \langle \hat{v}_5^\dagger \hat{c}_4 \rangle, \end{aligned} \quad (19)$$

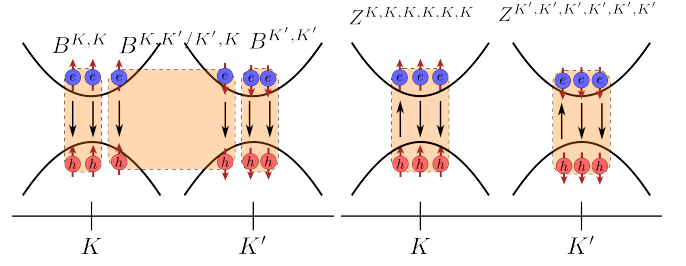


FIG. 2. Scheme of two-exciton transitions from Eq. (18) in the intravalley configuration $(K, K/K', K')$ and in the intervalley configuration $K, K'/K', K$ (left) and exciton-two-exciton transitions from Eq. (20) in the intravalley configuration (right).

which, after an exciton and exciton-two-exciton expansion, explicitly read:

$$\begin{aligned} Z_{\pm, \zeta, \mu, \nu, \mathbf{Q}}^{\xi_1, \xi_2, \xi_3, \xi_4, \xi_5, \xi_6} &= \sum_{\nu, \rho, \mathbf{Q}'} \Phi_{Z, \pm, \zeta, \mu, \nu, \rho, \mathbf{Q}'}^{*L, \xi_1, \xi_2, \xi_3, \xi_4, \xi_5, \xi_6}(\mathbf{Q}) \\ &\times \sum_{\eta, \lambda, \mathbf{Q}''} (S_{\pm}^{-1})_{\nu, \rho, \mathbf{Q}', \eta, \lambda, \mathbf{Q}''}^{\xi_3, \xi_4, \xi_5, \xi_6}(\mathbf{Q}) \sum_{\mathbf{q}} \varphi_{\mu, \mathbf{q} - \alpha_{\xi_2, \xi_1}}^{\xi_2, \xi_1} \mathbf{Q} \\ &\times \sum_{\mathbf{q}', \mathbf{q}''} \varphi_{\eta, \mathbf{q}' + \beta_{\xi_3, \xi_4/\xi_6}}^{* \xi_3, \xi_4/\xi_6} \varphi_{\lambda, \mathbf{q}'' - \alpha_{\xi_5, \xi_2/\xi_4}}^{* \xi_5, \xi_2/\xi_4} (\mathbf{Q} - \mathbf{Q}'') \\ &\times \frac{1}{2} \left(\langle \hat{c}_1^\dagger \hat{v}_2 \hat{v}_3^\dagger \hat{c}_4 \hat{v}_5^\dagger \hat{c}_6 \rangle_c \pm \langle \hat{c}_1^\dagger \hat{v}_2 \hat{v}_3^\dagger \hat{c}_4 \hat{v}_5^\dagger \hat{c}_6 \rangle_c \right), \end{aligned} \quad (20)$$

where $\Phi_{Z, \pm, \zeta, \mu, \nu, \rho, \mathbf{Q}'}^{*L, \xi_1, \xi_2, \xi_3, \xi_4, \xi_5, \xi_6}(\mathbf{Q})$ is the exciton-two-exciton wave function solving the exciton-two-exciton Schrödinger equation with quantum number ζ and configuration \pm , cf. Eq. (S19). We use the term “exciton-two-exciton transition” to generally denote all bound and unbound exciton-two-exciton states, while we use the term “exciton-two-exciton continuum”, if we specifically designate the continuum states, and we use the term “bound exciton-biexciton”, if we specifically designate the bound exciton-two-exciton state. Note, that the exciton-two-exciton transition is a different many-body correlation than a triexciton, as described in Refs. [84, 85], which is at least relevant in a fifth-order response. Also note, that the main difference to the two-exciton transitions B in Eq. (18) is the additional center-of-mass- \mathbf{Q} -dependence, i.e., the exciton-two-exciton transition carries a total momentum of $2\mathbf{Q}$ (excitonic center-of-mass momentum), as their source is of partly incoherent nature. Also note, that there is some ambiguity in the interpretation of Eq. (20), since $Z \sim \langle \hat{c}_1^\dagger \hat{v}_2 \hat{v}_3^\dagger \hat{c}_4 \hat{v}_5^\dagger \hat{c}_6 \rangle_c$ can be equally interpreted as a correlated coherence between an excitonic transition and a two-exciton transition $\langle (\hat{c}_1^\dagger \hat{v}_2)(\hat{v}_3^\dagger \hat{c}_4 \hat{v}_5^\dagger \hat{c}_6) \rangle_c$ or as an occupation-assisted excitonic transition $\langle (\hat{c}_1^\dagger \hat{v}_2 \hat{v}_3^\dagger \hat{c}_4)(\hat{v}_5^\dagger \hat{c}_6) \rangle_c$. However, both of these contributions are taken into account.

Throughout this work, we disregard correlated eight-operator expectation values of order $n = 4$ (quadrupole)

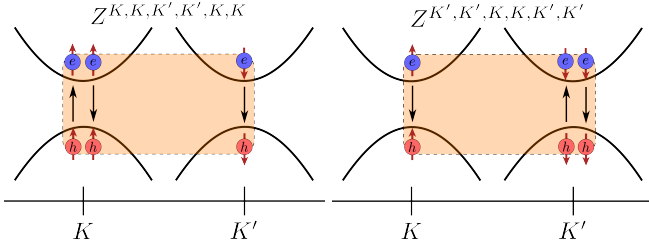


FIG. 3. Scheme of exciton-two-exciton transitions from Eq. (20) in the two possible intervalley configurations.

- P – Excitonic transition
- N – Excitonic occupation/intraexcitonic coherence
- B – Two-exciton transition
- Z – Exciton-two-exciton transition

TABLE I. Excitonic quantities considered in this work.

plets), which are expected to induce excitonic incoherent Coulomb scattering in the sense of exciton-exciton collisions. While it has been shown, that Coulomb scattering in the electron-hole picture beyond the Hartree-Fock limit [86] significantly suppresses Rabi oscillations in GaAs QWs, they can be recovered if the electron and hole occupation dynamics are formulated in a dressed-state basis [87]. This is the reason, why the semiconductor Bloch equations applied to material systems with weak Coulomb interaction already in Hartree-Fock limit successfully reproduced actual measured Rabi oscillations [6, 8]. Therefore, the neglect of incoherent Coulomb scattering in the study of Rabi oscillations in confined semiconductors such as conventional GaAs-like QWs, where light-matter interaction is of similar strength compared to Coulomb interaction, is justified as a first approximation. Future studies might shed more light on this issue.

We note, that Figs. 1–3 only display a selection of possible configurations, as we restrict the visualization to spin-bright A excitons, which are the primary focus of this manuscript. However, the excitonic theory developed here is equally able to resolve spin-dark A and spin-bright/spin-dark B excitons.

In Tab. I, we summarize all excitonic quantities considered in this work.

First-Order Contributions

In first order $m = 1$, which is the regime of linear optics, only excitonic transitions P_μ^ξ occur:

$$i\hbar\partial_t P_\mu^\xi \Big|_{\mathbf{E}^1} = (E_\mu^\xi - \hbar\omega_P - i\hbar\gamma_{\text{nr}}) P_\mu^\xi - \hbar\Omega^{cv,\xi} \sum_{\mathbf{q}} \varphi_{\mu,\mathbf{q}}^{*\xi,\xi}. \quad (21)$$

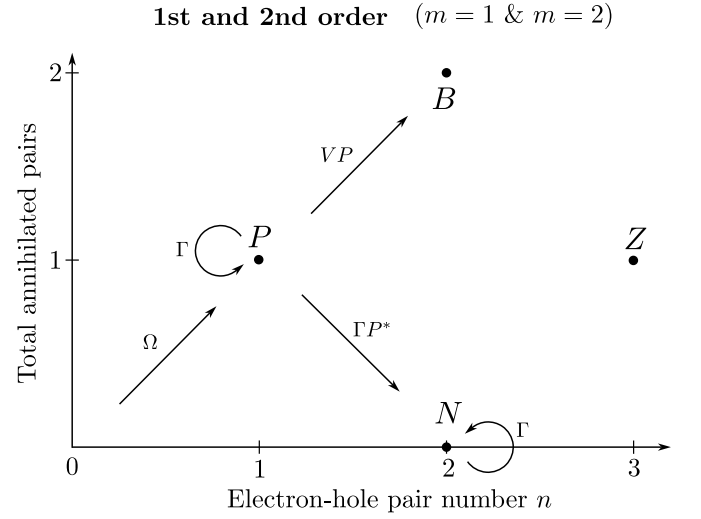


FIG. 4. Scheme of the interaction processes via optical ($\Omega \triangleq \Omega^{cv}$) and Coulomb (V) interaction up to second order DCT for the correlated expectation values in our theory. Additionally, we depict the exciton-phonon interaction in second-order Born-Markov approximation (Γ)

Here, $E_\mu^\xi = E_{\mu,\mathbf{Q}=0}^\xi$ is the excitonic energy with excitonic quantum number μ at zero center-of-mass momentum \mathbf{Q} and spin-valley index ξ , $\hbar\omega_P$ is the center frequency of the exciting optical pulse in a rotating frame, γ_{nr} is the total non-radiative homogeneous dephasing $\gamma_{\text{nr}} = \gamma_{\text{X-phon}} + \gamma_{\text{res}}$ by exciton-phonon interaction $\gamma_{\text{X-phon}}$ [88, 89], cf. circled arrow denoted by “ Γ ” in Fig. 4, and by other residual contributions γ_{res} via, e.g., scattering with uniformly distributed impurities [90, 91]. Inhomogeneous contributions are not considered, as their evaluation entails an ensemble average over many spatially dependent and randomly fluctuating slab- [92, 93] or substrate thicknesses [94] or non-uniformly distributed impurities, which greatly increases the numerical complexity. $\hbar\Omega^{cv} = (\hbar\Omega^{vc})^*$ is the Rabi energy:

$$\hbar\Omega^{cv,\xi}(t) = \frac{\mathbf{d}^{cv,\xi} \cdot \mathbf{E}^{\sigma\pm}}{2}, \quad (22)$$

with transition dipole moment $\mathbf{d}^{cv,\xi}$ [64, 95, 96] and optical field in circular basis in rotating wave approximation:

$$\mathbf{E}^{\sigma\pm}(t) = \mathbf{e}_\pm \tilde{E}(t), \quad (23)$$

with Jones vectors \mathbf{e}_\pm and Gaussian envelope:

$$\tilde{E}(t) = \frac{E_0}{\sqrt{2\pi}\sigma_P} e^{-\frac{t^2}{2\sigma_P^2}}, \quad (24)$$

where σ_P is the pulse duration determined by the intensity FWHM:

$$\sigma_P = \frac{\text{FWHM}}{2\sqrt{\ln(2)}}. \quad (25)$$

To keep the parameter set as small as possible, we introduce the pulse area Θ as a tuning knob of the optical excitation strength:

$$\Theta = \int_{-\infty}^{\infty} dt \Omega^{cv}(t), \quad (26)$$

and neglect any contributions due to reradiation [63].

Throughout the manuscript, we assume normal incidence with $\mathbf{E}_Q = \mathbf{E}\delta_{Q,0}$, i.e., we always assume spatial in-plane homogeneity and neglect any diffusion [97, 98], as such effect is negligible during the ultrafast timescales considered in this manuscript [99–102].

In Fig. 4, we depict the action of the optical pulse (Ω) annihilating an excitonic transition P in first order and the coupling to B and N in second order: Here, the y -axis denotes the total annihilated electron-hole pairs described by the corresponding correlation P , B , N etc. and the x -axis denotes the total electron-hole pair number n , cf. also Eq. (11). Note again, that – in contrast to, e.g., Refs. [22, 24, 25] – we always use the correlated excitonic operator expectation values throughout this work.

Second-Order Contributions

In second order $m = 2$, the equations of motion for the excitonic occupations/intraexcitonic coherences read:

$$i\hbar\partial_t N_{\sigma,\lambda,Q}^{\xi,\xi'} \Big|_{\mathbf{E}^2} = \left(E_{\lambda,Q}^{\xi,\xi'} - E_{\sigma,Q}^{\xi,\xi'} \right) N_{\sigma,\lambda,Q}^{\xi,\xi'} + i\hbar\partial_t N_{\sigma,\lambda,Q}^{\xi,\xi'} \Big|_{\mathbf{E}^2, \text{X-phon}}, \quad (27)$$

where the first line denotes the free excitonic contribution. We note, that, on this level, exciton-phonon interaction (second line in Eq. (27)) provides an additional important contribution, which, in second-order Born-Markov approximation, can be written as [42, 43, 103]:

$$i\hbar\partial_t N_{\sigma,\lambda,Q}^{\xi,\xi'} \Big|_{\mathbf{E}^2, \text{X-phon}} = \sum_{\mu,\nu,\mathbf{K}} \Gamma_{\sigma,\lambda,Q,\mu,\nu,0,-\mathbf{Q}}^{\text{in},\xi,\xi'} P_{\mu}^* P_{\nu}^{\xi} + \sum_{\mu,\nu,\mathbf{K}} \left(\Gamma_{\sigma,\lambda,Q,\mu,\nu,\mathbf{Q}+\mathbf{K},\mathbf{K}}^{\text{in},\xi,\xi'} N_{\mu,\nu,\mathbf{Q}+\mathbf{K}}^{\xi,\xi'} - \Gamma_{\sigma,\lambda,Q,\mu,\nu,\mathbf{Q}+\mathbf{K},\mathbf{K}}^{\text{out},\xi,\xi'} N_{\sigma,\lambda,Q}^{\xi,\xi'} \right). \quad (28)$$

Here, the first line denotes the phonon-assisted formation of excitonic occupations/intraexcitonic coherences, process " ΓP^* " in Fig. 4, while the remaining terms denote phonon-assisted scattering and thermalization, process " Γ " denoted by a circled arrow. The phonon-assisted scattering rates $\Gamma^{\text{in/out}}$ can be deduced from, e.g., Refs. [42, 43]. Since we focus on light-matter- and Coulomb interaction at elevated densities during intense optical fields beyond the $\chi^{(3)}$ -limit, we neglect incoherent exciton-phonon scattering in the following. Nevertheless, we want to emphasize, that exciton-phonon scattering can become important in the incoherent limit at

nonlinear exciton densities. For a detailed analysis of the occurring fermionic, bosonic and exchange contributions we refer to Refs. [45, 47]. Direct optical-field pump-contributions to the excitonic occupations/intraexcitonic coherences, denoted by " Ω ", vanish: $i\hbar\partial_t N_{\sigma,\lambda,Q}^{\xi,\xi'} \Big|_{\mathbf{E}^2, \Omega} = 0$. Note, that if we additionally considered intraband light-matter interaction [66], intraexcitonic coherences and excitonic drift can occur already in second-order via, e.g., terahertz fields [69, 104, 105].

The equations of motion for the two-exciton transitions read [17, 18, 82]:

$$i\hbar\partial_t B_{\pm,\zeta}^{\xi,\xi'} \Big|_{\mathbf{E}^2} = \left(E_{B,\pm,\zeta}^{\xi,\xi'} - i\hbar\gamma_B \right) B_{\pm,\zeta}^{\xi,\xi'} + \frac{1}{2} \sum_{\sigma,\eta,\mathbf{K}} \Phi_{B,\pm,\zeta,\sigma,\eta,\mathbf{K}}^{*L,\xi,\xi,\xi',\xi'} \sum_{\rho,\lambda,\mathbf{Q}} (S^{-1})_{\sigma,\eta,\mathbf{K},\rho,\lambda,\mathbf{Q}}^{\xi,\xi,\xi',\xi'} (0) \times \sum_{\mu,\nu} \left(V_{1,\rho,\lambda,\mathbf{Q},\mu,\nu,0}^{\xi,\xi,\xi',\xi'} \mp V_{2,\rho,\lambda,\mathbf{Q},\mu,\nu,0}^{\xi,\xi,\xi',\xi'} (0) \right) \times P_{\mu}^{\xi} P_{\nu}^{\xi'} (\delta_{\xi,\xi'} \pm 1). \quad (29)$$

Here, $E_{B,\pm,\zeta}^{\xi,\xi'}$ is the two-exciton dispersion with two-exciton quantum number ζ , configuration \pm and two-exciton dephasing γ_B , which we set as $\gamma_B = 2\gamma_{\text{nrad}}$. Note, that the dephasing of bound biexcitons can differ from this assumption [106]. $\Phi_{B,\pm,\zeta,\sigma,\eta,\mathbf{K}}^{*L,\xi,\xi,\xi',\xi'}$ is the two-exciton wave function as a solution of the two-exciton Schrödinger equation in Eq. (S18), S is the projection matrix in Eq. (S23) and V_1 and V_2 are exciton-exciton matrix elements, cf. Eq. (S24) and Eq. (S25). The "+" configuration, which can occur within equal valleys $\xi = \xi'$ or distinct valleys $\xi \neq \xi'$, hosts only continuum states. In contrast, the "−" configuration, where only two excitonic transitions from different spin-valleys $\xi \neq \xi'$ are involved, as the contribution within equal valleys $\xi = \xi'$ vanishes, hosts one bound state, the bound biexciton, and a continuum. In general, two-exciton transitions are induced via a product of two excitonic transitions P via the exciton-exciton scattering encoded in the matrix elements $V_{1/2}$. The corresponding process is depicted in Fig. 4 via " VP ".

We note, that at this level, no impact of two-exciton transitions or excitonic occupations/intraexcitonic coherences on the optical response occurs, as the two-exciton transitions B and the excitonic occupations/intraexcitonic coherences N do not couple back to the excitonic transitions P , cf. Fig. 4. However, at this level, exciton dynamics can still be calculated, if exciton-phonon interaction is considered. Since there is no interaction between excitonic occupations/intraexcitonic coherences and two-exciton transitions, the exciton dynamics are purely bosonic up to second order.

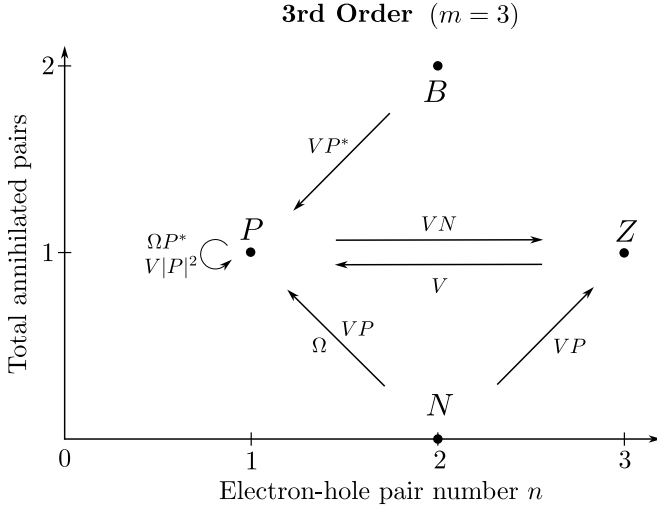


FIG. 5. Scheme of the interaction processes via optical ($\Omega \triangleq \Omega^{cv}$) and Coulomb (V) interaction on third order DCT for the correlated expectation values considered in our theory.

Third-Order Contributions

In third order in the optical field $m = 3$, the following contributions to the excitonic transition need to be distinguished: Fully coherent contributions (COH), correlated contributions (CORR) and exciton-exciton (XX) contributions. Fully coherent (COH) contributions only involve products of the excitonic transitions P , correlated contributions (CORR) involve products of excitonic occupations/intraexcitonic coherences N , i.e., they constitute correlated coherent (intraexcitonic coherences) or fully incoherent (excitonic occupations) contributions, and exciton-exciton (XX) contributions involve coherent two-exciton transitions B and coherent-incoherent exciton-two-exciton transitions Z . In Fig. 5, we depict all interaction processes in third order schematically.

The fully coherent contributions to the excitonic transition P read:

$$\begin{aligned} i\hbar\partial_t P_\mu^\xi \Big|_{\mathbf{E}^3, \text{COH}} &= \sum_{\nu, \rho, \eta} \frac{1}{2} \left(U_{3, \mu, \nu, \rho, \eta, \mathbf{0}}^{\xi, \xi} + U_{4, \mu, \nu, \rho, \eta, \mathbf{0}}^{\xi, \xi} \right) P_\rho^* P_\eta^\xi P_\nu^\xi \\ &+ \hbar\Omega^{cv, \xi} \sum_{\nu, \rho} \left(D_{1, \mu, \nu, \rho, \mathbf{0}}^{\xi, \xi} + D_{2, \mu, \nu, \rho, \mathbf{0}}^{\xi, \xi} \right) P_\nu^* P_\rho^\xi, \quad (30) \end{aligned}$$

where the first line encodes coherent band-gap reduction and excitonic phase-space filling, cf. process " $V|P|^2$ " in Fig. 5, mediated via the Coulomb matrix element $U_{3/4}$, cf. Eq. (S40) and Eq. (S41), and the second line describes coherent Pauli-blocking, cf. process " ΩP^* " in Fig. 5, via the matrix elements $D_{1/2}$, cf. Eq. (S28) and Eq. (S29). Note, that the coherent Pauli-blocking term can also be viewed as a light-induced dressing contribution, since we can always factor out one excitonic transition P .

The contributions to the excitonic transition P due to excitonic occupations and intraexcitonic coherences read:

$$\begin{aligned} i\hbar\partial_t P_\mu^\xi \Big|_{\mathbf{E}^3, \text{CORR}} &= \sum_{\nu, \rho, \eta, \mathbf{Q}} U_{2, \mu, \nu, \rho, \eta, \mathbf{Q}}^{\xi, \xi} N_{\rho, \eta, \mathbf{Q}}^{\xi, \xi} P_\nu^\xi \\ &+ \sum_{\nu, \rho, \eta, \mathbf{Q}, \xi'} \left(U_{3, \mu, \nu, \rho, \eta, \mathbf{Q}}^{\xi, \xi'} N_{\rho, \eta, \mathbf{Q}}^{\xi, \xi'} + U_{4, \mu, \nu, \rho, \eta, \mathbf{Q}}^{\xi', \xi} N_{\rho, \eta, \mathbf{Q}}^{\xi', \xi} \right) P_\nu^\xi \\ &+ \hbar\Omega^{cv} \sum_{\mathbf{Q}, \nu, \rho, \xi'} \left(D_{1, \mu, \nu, \rho, \mathbf{Q}}^{\xi, \xi'} N_{\nu, \rho, \mathbf{Q}}^{\xi, \xi'} + D_{2, \mu, \nu, \rho, \mathbf{Q}}^{\xi', \xi} N_{\nu, \rho, \mathbf{Q}}^{\xi', \xi} \right), \quad (31) \end{aligned}$$

where the first two lines encode incoherent band-gap reduction and excitonic phase-space filling, cf. process " VP " denoted by an arrow from N to P in Fig. 5, mediated via the Coulomb matrix element $U_{2/3/4}$, cf. Eqs. (S39)–(S41), the third line describes incoherent Pauli-blocking, cf. process " Ω " in Fig. 5, via the matrix elements $D_{1/2}$, cf. Eq. (S28) and Eq. (S29).

The exciton-exciton contributions read:

$$\begin{aligned} i\hbar\partial_t P_\mu^\xi \Big|_{\mathbf{E}^3, \text{XX}} &= \sum_{\nu, \rho, \lambda, \mathbf{Q}, \xi', \zeta, \pm} \left(\pm \left(V_{1, \rho, \lambda, \mathbf{Q}, \mu, \nu, \mathbf{0}}^{\xi, \xi', \xi'} \right)^* - \left(V_{2, \rho, \lambda, \mathbf{Q}, \mu, \nu, \mathbf{0}}^{\xi, \xi', \xi'}(\mathbf{0}) \right)^* \right) \\ &\quad \times \Phi_{\pm, \zeta, \rho, \lambda, \mathbf{Q}}^{\text{R}, \xi, \xi', \xi'}(\mathbf{0}) B_{\pm, \zeta}^{\xi, \xi'} P_\nu^* \\ &+ \sum_{\nu, \rho, \lambda, \mathbf{Q}, \mathbf{Q}', \xi', \xi'', \zeta, \pm} \left(\pm \left(V_{1, \rho, \lambda, \mathbf{Q}, \mu, \nu, \mathbf{0}}^{\xi, \xi', \xi''} \right)^* - \left(V_{2, \rho, \lambda, \mathbf{Q}, \mu, \nu, \mathbf{0}}^{\xi, \xi', \xi''}(\mathbf{Q}) \right)^* \right) \\ &\quad \times \Phi_{\pm, \zeta, \rho, \lambda, \mathbf{Q}'}^{\text{R}, \xi, \xi', \xi''}(\mathbf{Q}) Z_{\pm, \zeta, \nu, \mathbf{Q}}^{\xi'', \xi', \xi, \xi', \xi''} \quad (32) \end{aligned}$$

where the first two lines describe the interaction with two-exciton transitions B , cf. processes " VP^* " in Fig. 5, and the last two lines describe the interaction with exciton-two-exciton transitions Z , cf. processes " V " with the exciton-exciton matrix elements $V_{1/2}$, cf. Eq. (S24) and Eq. (S25).

Also, in third order, the equations of motion for the exciton-two-exciton transitions Z occur:

$$\begin{aligned} i\hbar\partial_t Z_{\pm, \zeta, \rho, \mathbf{Q}}^{\xi_1, \xi_2, \xi_3, \xi_4, \xi_5, \xi_6} \Big|_{\mathbf{E}^3} &= \left(E_{R, \pm, \zeta, \rho, \mathbf{Q}}^{\xi_1, \xi_2, \xi_3, \xi_4, \xi_5, \xi_6} - i\hbar\gamma_Z \right) \\ &\times Z_{\pm, \zeta, \rho, \mathbf{Q}}^{\xi_1, \xi_2, \xi_3, \xi_4, \xi_5, \xi_6} + \frac{1}{2} \sum_{\mu, \delta, \mathbf{K}} \Phi_{R, \pm, \zeta, \mu, \delta, \mathbf{K}}^* L_{\xi_3, \xi_4, \xi_5, \xi_6}(\mathbf{Q}) \\ &\times \sum_{\lambda, \sigma, \mathbf{Q}'} (S_{\pm}^{-1})_{\mu, \delta, \mathbf{K}, \lambda, \sigma, \mathbf{Q}'}^{\xi_3, \xi_4, \xi_5, \xi_6}(\mathbf{Q}) \\ &\times \sum_{\nu} \left(\left(V_{1, \lambda, \sigma, \mathbf{Q}', \nu, \rho, \mathbf{0}}^{\xi_3, \xi_4, \xi_5, \xi_6} \mp V_{4, \lambda, \sigma, \mathbf{Q}', \nu, \rho, \mathbf{Q}}^{\xi_3, \xi_4, \xi_5, \xi_6} \right) \right. \\ &\quad \times P_\nu^{\xi_3} (\delta_{\xi_3, \xi_6} \delta_{\xi_1, \xi_4} \pm \delta_{\xi_3, \xi_4} \delta_{\xi_1, \xi_6}) \delta_{\xi_2, \xi_5} \\ &\quad \left. + \left(V_{1, \lambda, \sigma, \mathbf{Q}', \nu, \rho, \mathbf{Q}}^{\xi_3, \xi_4, \xi_5, \xi_6} \mp V_{3, \lambda, \sigma, \mathbf{Q}', \nu, \rho, \mathbf{Q}}^{\xi_3, \xi_4, \xi_5, \xi_6} \right) \right) \\ &\times P_\nu^{\xi_5} (\delta_{\xi_5, \xi_4} \delta_{\xi_1, \xi_6} \pm \delta_{\xi_5, \xi_6} \delta_{\xi_1, \xi_4}) \delta_{\xi_2, \xi_3} N_{\rho, \mathbf{Q}}^{\xi_2, \xi_1}. \quad (33) \end{aligned}$$

Here, $E_{R,\pm,\zeta,\rho,\mathbf{Q}}^{\xi_1,\xi_2,\xi_3,\xi_4,\xi_5,\xi_6}$ is the exciton-two-exciton dispersion for configuration \pm , exciton-two-exciton quantum number ζ , momentum \mathbf{Q} and γ_Z is the exciton-biexciton dephasing, which we set as $\gamma_Z = 3\gamma_{\text{nrad}}$. Note, that the dephasing of the bound exciton-biexciton may differ from this assumption [106]. Similar to Eq. (18), the "+" configuration, which exists for intra- and intervalley configurations, hosts exciton-two-exciton continuum states, while the "-" configuration, which vanishes for intravalley interactions, hosts one bound state and a continuum. The main difference to the two-exciton transitions in Eq. (18) is, that the exciton-two-exciton transitions exhibit a partly incoherent nature, as they are induced by a product of intraexcitonic coherences/excitonic occupations $N_{\mathbf{Q}}$ and excitonic transitions P mediated via the exciton-exciton matrix elements $V_{1/3/4}$. The corresponding process "VN" is denoted by an arrow from P to Z . We note, that "VP", denoted by an arrow from N to Z in Fig. 5 denotes the same process, but from a different viewpoint. For that matter, the exciton-two-exciton wave functions $\Phi_{R,\pm,\zeta;\mu,\delta,\mathbf{K}}^{*L,\xi_3,\xi_4,\xi_5,\xi_6}(\mathbf{Q})$ solving the exciton-two-exciton Schrödinger equation in Eq. (S19) acquire an additional dependence on the center-of-mass momentum \mathbf{Q} corresponding to the exciton-two-exciton-inducing intraexcitonic coherence/incoherent excitonic occupation $N_{\mathbf{Q}}$. The exciton-exciton matrix elements $V_{1/3/4}$ entering Eq. (33) are given in Eq. (S24), Eq. (S26) and Eq. (S27), respectively.

Compared to second order, incoherent occupations/intraexcitonic coherences and two-exciton transitions couple back to the excitonic transitions via many-body optical and/or Coulomb interaction processes, cf. Fig. 5. Additionally, the partially incoherent exciton-two-exciton transitions, cf. Eq. (20), which emerge in third order, cf. Eq. (33), and, at the same time, couple back to the excitonic transitions, cf. Eq. (32), serve as an important bridge between the coherent and incoherent dynamics. In particular, in two-pulse pump-probe experiments, they adopt the role of the fully coherent two-exciton transitions B in Eq. (18), when all pump-induced coherent excitonic transitions P have been decayed and the system is in a fully incoherent state $N_{\mathbf{Q}}$. Hence, if we combine the equations of motion up to third order with exciton-phonon scattering (and density-independent Coulomb scattering such as intervalley exchange [52, 53, 56, 57] or Dexter interaction [59, 60]), a comprehensive description of pump-probe experiments from the coherent to the incoherent regime valid for small to moderate pump fluences can be obtained.

Fourth-Order Contributions

To investigate the optical response beyond the limit of third-order nonlinearities, we have to consider contributions up to the fourth order in the optical field $m = 4$.

Next to the distinction in fully coherent (COH), correlated (CORR) and exciton-exciton (XX) contributions,

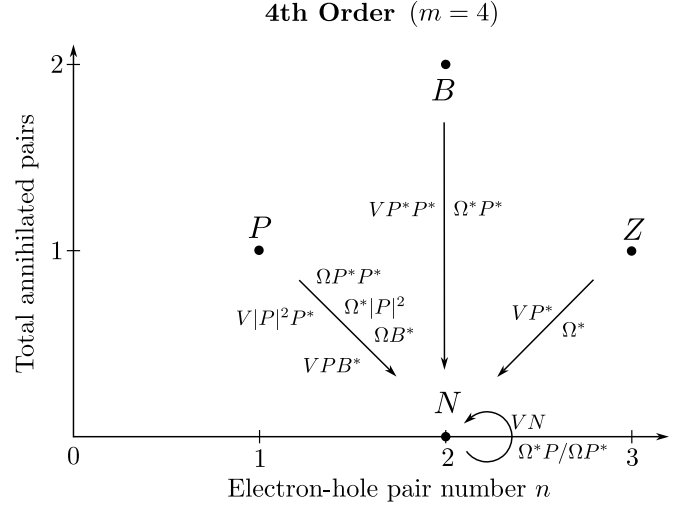


FIG. 6. Scheme of the interaction processes via optical ($\Omega \triangleq \Omega^{cv}$) and Coulomb (V) interaction on fourth order DCT for the correlated expectation values considered in our theory. Note, that we exclude correlated eight-operator expectation values and fourth-order optical and Coulomb contributions to the biexcitons B .

which we introduced in third order, we additionally group the equations in optical interaction (Ω) and Coulomb interaction (V).

In Fig. 6, we schematically depict all fourth-order interaction processes considered in this manuscript.

The fully coherent contributions to the intraexcitonic coherences/excitonic occupations $N_{\mathbf{Q}}$ via optical interaction read, cf. process "ΩP*P*" in Fig. 6:

$$i\hbar\partial_t N_{\sigma,\lambda,\mathbf{Q}}^{\xi,\xi'} \Big|_{\mathbf{E}^4,\Omega,\text{COH}} = \sum_{\mu,\nu,\eta} \left(\hbar\Omega^{vc,\xi} D_{3,\sigma,\lambda,\mu,\nu,\eta}^{\xi,\xi'} P_{\mu}^{*\xi} + \hbar\Omega^{vc,\xi'} D_{4,\sigma,\lambda,\mu,\nu,\eta}^{\xi,\xi'} P_{\nu}^{*\xi'} P_{\eta}^{\xi} - (\sigma \leftrightarrow \lambda)^* \right), \quad (34)$$

which describes the coherent excitation of intraexcitonic coherences/excitonic occupations $N_{\mathbf{Q}}$ via coherent excitonic transitions P mediated by the Pauli-blocking matrix elements $D_{3/4}$, cf. Eq. (S30) and Eq. (S31). While optical excitation at normal incidence with $\mathbf{E}_{\mathbf{Q}} = \mathbf{E}\delta_{\mathbf{Q},0}$ only excites coherent excitonic transitions at $\mathbf{Q} = 0$ (and a certain distribution of relative momenta $\mathbf{q} \geq 0$), cf. Eq. (21), interactions in fourth order of the optical field in Eq. (34) cause the coherent excitation of excitonic occupations with a certain center-of-mass distribution out of the light cone $\mathbf{Q} \geq 0$. This behavior can be understood via the fermionic substructure, as individual electron and hole collisions via Coulomb interaction redistribute the center-of-mass momenta \mathbf{Q} and relative momenta within the exciton gas. These individual electron and hole collisions are encoded in the many-body matrix elements $D_{3/4}$.

Moreover, contributions to intraexcitonic coherences/excitonic occupations $N_{\mathbf{Q}}$ via optical interaction beyond the fully coherent limit occur, cf. process

" $\Omega^*P/\Omega P^*$ " in Fig. 6:

$$\begin{aligned}
i\hbar\partial_t N_{\sigma,\lambda,\mathbf{Q}}^{\xi,\xi'} \Big|_{\mathbf{E}^4,\Omega,\text{CORR}} = & - \sum_{\mu,\nu} \left(\hbar\Omega^{vc,\xi} D_{1,\mu,\sigma,\nu,\mathbf{Q}}^{*,\xi,\xi'} P_{\mu}^{\xi} \right. \\
& \left. + \hbar\Omega^{vc,\xi'} D_{2,\mu,\sigma,\nu,\mathbf{Q}}^{*,\xi,\xi'} P_{\mu}^{\xi'} \right) N_{\nu,\lambda,\mathbf{Q}}^{\xi,\xi'} \\
& + \sum_{\mathbf{Q}',\mu,\nu,\eta} \hbar\Omega^{vc,\xi} D_{5,\sigma,\lambda,\mu,\nu,\eta,\mathbf{Q},\mathbf{Q}'}^{\xi} P_{\mu}^{\xi} N_{\nu,\eta,\mathbf{Q}'}^{\xi,\xi} \delta_{\xi,\xi'} \\
& + \sum_{\mathbf{Q}',\mu,\nu,\eta,\xi''} \left(\hbar\Omega^{vc,\xi} D_{6,\sigma,\lambda,\mu,\nu,\eta,\mathbf{Q},\mathbf{Q}'}^{\xi,\xi'',\xi''} P_{\mu}^{\xi} N_{\nu,\eta,\mathbf{Q}'}^{\xi'',\xi'} \right. \\
& \left. + \hbar\Omega^{vc,\xi'} D_{7,\sigma,\lambda,\mu,\nu,\eta,\mathbf{Q},\mathbf{Q}'}^{\xi,\xi'',\xi''} P_{\mu}^{\xi'} N_{\nu,\eta,\mathbf{Q}'}^{\xi'',\xi''} \right) - (\sigma \leftrightarrow \lambda)^*. \quad (35)
\end{aligned}$$

Here, the first two lines describe an attenuation of the coherent excitation of intraexcitonic coherences/excitonic occupations, as soon as excitonic states at equal center-of-mass momenta are occupied, mediated by the Pauli-blocking matrix elements $D_{1/2}$, cf. Eq. (S28) and Eq. (S29). The last three lines describe a build-up of the coherent excitation of intraexcitonic coherences/excitonic occupations at COM momentum \mathbf{Q} in the presence of intraexcitonic coherences/excitonic occupations at all other COM momenta \mathbf{Q}' via intravalley (third line) or intervalley correlations (fourth and fifth line) via the many-body matrix elements $D_{5/6/7}$, cf. Eqs. (S32)–(S34).

Additionally, Coulomb interaction induces a coherent excitation of intraexcitonic coherences, cf. process " $V|P|^2P$ " in Fig. 6:

$$\begin{aligned}
i\hbar\partial_t N_{\sigma,\lambda,\mathbf{Q}}^{\xi,\xi'} \Big|_{\mathbf{E}^4,V,\text{COH}} = & \sum_{\mu,\nu,\rho,\eta} P_{\mu}^{*\xi} P_{\nu}^{\xi} P_{\rho}^{*\xi'} P_{\eta}^{\xi'} \\
& \times \left(U_{5,\sigma,\lambda,\mu,\nu,\rho,\eta,\mathbf{Q}}^{\xi} \delta_{\xi,\xi'} + U_{6,\sigma,\lambda,\mu,\nu,\rho,\eta,\mathbf{Q}}^{\xi,\xi'} \right) - (\sigma \leftrightarrow \lambda)^*, \quad (36)
\end{aligned}$$

in the presence of excitonic transitions P mediated via the coupling elements $U_{5/6}$, cf. Eq. (S42) and Eq. (S43). If only excitonic transitions P_{μ} of a single excitonic state $\mu = \nu = \rho = \eta$ are present, this contribution vanishes for excitonic occupations with $\sigma = \lambda$:

$$i\hbar\partial_t N_{\sigma,\sigma,\mathbf{Q}}^{\xi,\xi'} \Big|_{\mathbf{E}^4,V,\text{COH}} = 0, \quad (37)$$

while intraexcitonic coherences with $\sigma \neq \lambda$ can still be induced:

$$i\hbar\partial_t N_{\sigma,\lambda,\mathbf{Q}}^{\xi,\xi'} \Big|_{\mathbf{E}^4,V,\text{COH}} \neq 0. \quad (38)$$

For excitonic transitions of an arbitrary admixture of states, intraexcitonic coherences with $\sigma \neq \lambda$ and also excitonic occupations with $\mu = \lambda$ are induced.

Beyond a fully coherent limit, Coulomb interaction causes a coupling between intraexcitonic coherences and

excitonic occupations, cf. process " VN " in Fig. 6:

$$\begin{aligned}
i\hbar\partial_t N_{\sigma,\lambda,\mathbf{Q}}^{\xi,\xi'} \Big|_{\mathbf{E}^4,V,\text{CORR}} = & \sum_{\mu,\nu,\rho,\eta,\mathbf{Q}'} \left(U_{7,\sigma,\lambda,\mu,\nu,\rho,\eta,\mathbf{Q},\mathbf{Q}'}^{\xi,\xi'} N_{\mu,\nu,\mathbf{Q}}^{\xi,\xi'} \overline{N_{\rho,\eta,\mathbf{Q}'}^{\xi,\xi'}} \right. \\
& + \sum_{\xi''} U_{8,\sigma,\lambda,\mu,\nu,\rho,\eta,\mathbf{Q},\mathbf{Q}'}^{\xi,\xi',\xi''} N_{\mu,\nu,\mathbf{Q}}^{\xi,\xi'} \overline{N_{\rho,\eta,\mathbf{Q}'}^{\xi'',\xi'}} \\
& + \sum_{\xi''} U_{9,\sigma,\lambda,\mu,\nu,\rho,\eta,\mathbf{Q},\mathbf{Q}'}^{\xi,\xi',\xi''} N_{\mu,\nu,\mathbf{Q}}^{\xi,\xi'} \overline{N_{\rho,\eta,\mathbf{Q}'}^{\xi,\xi''}} \\
& + \sum_{\mathbf{Q}'',\xi''} U_{10,\sigma,\lambda,\mu,\nu,\rho,\eta,\mathbf{Q},\mathbf{Q}',\mathbf{Q}''}^{\xi,\xi',\xi''} \overline{N_{\mu,\nu,\mathbf{Q}'}^{\xi,\xi'}} N_{\rho,\eta,\mathbf{Q}''}^{\xi'',\xi'} \\
& + \sum_{\mathbf{Q}'',\xi''} U_{11,\sigma,\lambda,\mu,\nu,\rho,\eta,\mathbf{Q},\mathbf{Q}',\mathbf{Q}''}^{\xi,\xi',\xi''} \overline{N_{\mu,\nu,\mathbf{Q}'}^{\xi,\xi'}} N_{\rho,\eta,\mathbf{Q}''}^{\xi,\xi''} \\
& + \sum_{\mathbf{Q}'',\xi''} U_{12,\sigma,\lambda,\mu,\nu,\rho,\eta,\mathbf{Q},\mathbf{Q}',\mathbf{Q}''}^{\xi,\xi',\xi''} \overline{N_{\mu,\nu,\mathbf{Q}'}^{\xi,\xi'}} N_{\rho,\eta,\mathbf{Q}''}^{\xi,\xi'} \\
& \left. + \sum_{\mathbf{Q}'',\xi'',\xi'''} U_{13,\sigma,\lambda,\mu,\nu,\rho,\eta,\mathbf{Q},\mathbf{Q}',\mathbf{Q}'',\mathbf{Q}'''}^{\xi,\xi',\xi'',\xi'''} \overline{N_{\mu,\nu,\mathbf{Q}'}^{\xi,\xi'}} N_{\rho,\eta,\mathbf{Q}''}^{\xi'',\xi'''} N_{\rho,\eta,\mathbf{Q}'''}^{\xi,\xi'''} \right) \\
& - (\sigma \leftrightarrow \lambda)^*, \quad (39)
\end{aligned}$$

mediated by the exciton-exciton matrix elements $U_{7/8/9/10/11/12/13}$, cf. Eqs. (S44)–(S50). In Eq. (39), we use a short-hand notation as follows:

$$\overline{N_{\mu,\nu,\mathbf{Q}}^{\xi,\xi'}} = N_{\mu,\nu,\mathbf{Q}}^{\xi,\xi'} + P_{\mu}^{*\xi} P_{\nu}^{\xi} \delta_{\mathbf{Q},\mathbf{0}}^{\xi,\xi'}, \quad (40)$$

and:

$$\begin{aligned}
\overline{N_{\mu,\nu,\mathbf{Q}}^{\xi,\xi'} N_{\rho,\eta,\mathbf{Q}'}^{\xi'',\xi'''}} = & N_{\mu,\nu,\mathbf{Q}}^{\xi,\xi'} N_{\rho,\eta,\mathbf{Q}'}^{\xi'',\xi'''} \\
& + N_{\mu,\nu,\mathbf{Q}}^{\xi,\xi'} P_{\rho}^{*\xi''} P_{\eta}^{\xi''} \delta_{\mathbf{Q}',\mathbf{0}}^{\xi'',\xi'''} + N_{\rho,\eta,\mathbf{Q}'}^{\xi'',\xi'''} P_{\mu}^{*\xi} P_{\nu}^{\xi} \delta_{\mathbf{Q},\mathbf{0}}^{\xi,\xi'} \quad (41)
\end{aligned}$$

If we only consider diagonal excitonic occupations $\sigma = \lambda$, $\mu = \nu$ and $\rho = \eta$ on both sides, Eq. (39) vanishes:

$$i\hbar\partial_t N_{\sigma,\sigma,\mathbf{Q}}^{\xi,\xi'} \Big|_{\mathbf{E}^4,V,\text{CORR}} = 0. \quad (42)$$

Therefore, there does not exist a direct coupling between excitonic occupations, but excitonic occupations at quantum number μ can induce intraexcitonic coherences at quantum number μ, ν , which in turn couple back to excitonic occupations at quantum number ν creating potential excitonic oscillations. In Refs. [28, 29], similar expressions have been derived in the limit of vanishing center-of-mass momentum, where the interaction of excitonic occupations and intraexcitonic coherences involving higher-lying excitonic states has been shown to cause an oscillatory behavior in the 1s excitonic occupation in time.

At last, contributions, which describe the coupling between two-exciton transitions and exciton-two-exciton transitions via optical (Ω) and Coulomb (V) interaction, occur on fourth order. The optical interaction process,

cf. process " ΩB^* " denoted by an arrow from P to N or " $\Omega^* P^*$ " denoted by an arrow from B to N (both denote the same process) in Fig. 6, exhibits the following structure:

$$i\hbar\partial_t N_{\sigma,\lambda,\mathbf{Q}}^{\xi,\xi'} \Big|_{\mathbf{E}^4,\Omega,XX} \sim \hbar\Omega^{vc} P^* B + \hbar\Omega^{vc} Z - (\sigma \leftrightarrow \lambda)^* . \quad (43)$$

The Coulomb interaction process, cf. process " VPB^* " denoted by an arrow from P to N or " VP^*P^* " denoted by an arrow from B to N (both denote the same process) in Fig. 6, exhibits the following structure:

$$i\hbar\partial_t N_{\sigma,\lambda,\mathbf{Q}}^{\xi,\xi'} \Big|_{\mathbf{E}^4,V,XX} \sim VP^*P^*B + VP^*Z - (\sigma \leftrightarrow \lambda)^* . \quad (44)$$

Eq. (43) and Eq. (44) exhibit very lengthy expressions, so that we refer to Eq. (S66) and Eq. (S67) in the SM for their explicit forms. Again, similar to Eq. (34), Eq. (43) and Eq. (44) induce incoherent, optically dark excitonic occupations out of the light cone due to optical and Coulomb interaction processes via intermediate two-exciton transitions or exciton-two-exciton transitions. Similar contributions to the coherent formation of excitonic occupations outside the light cone at $\mathbf{Q} > \mathbf{0}$ have been found in Ref. [33], where a fully bosonic excitonic description has been applied. In particular, the fully coherent contributions in Eq. (44) (first terms $\sim P^*P^*B$) resemble the terms found in Ref. [33]. However, in our numerical simulations, it turns out, that the most important contributions to the coherent excitation of excitonic occupations out of the light cone are the fermionic Pauli-blocking contributions in Eq. (34) and Eq. (35). Eq. (44) constitute only minor corrections, which we found to *attenuate* rather than increase the overall coherently excited excitonic occupation out of the light cone. This observation is in line with the argumentation in Ref. [30], where similar expressions in a Wannier basis have been derived.

We note, that, in fourth order, additional contributions to the two-exciton transitions B with respect to optical interaction and Coulomb interaction appear. However, since we always eliminate the two-exciton and exciton-two-exciton continua within a Markov approximation in our simulations, these fourth-order contributions would yield equations of motion already beyond fourth order. Hence, we disregard them. Thus, a Markovian elimination of the two-exciton continua, cf. Eq. (29), and exciton-two-exciton continua, cf. Eq. (33), corresponds to a second-order Born approximation on third order DCT, but is already beyond a Born approximation in fourth-order DCT, as the coupling to the excitonic occupations/intraexcitonic coherences N contains mixed light-matter and Coulomb interaction contributions. Hence, a second-order Born approximation is only exact up to third-order DCT, as a fourth-order DCT gives rise to mixed interactions.

Moreover, in a full treatment without a Markovian elimination, the additionally appearing fourth-order

terms in the equations of motion of B give rise to optical Pauli-blocking and Coulomb energy renormalizations of the biexcitons and a coupling between biexcitons B and biexcitonic occupations, if correlated eight-operator expectation values are explicitly considered as well. These contributions could be necessary to explain power-dependent biexcitonic photoluminescence signatures [107] opening up the possibility of a theoretical understanding of the biexciton gain [108]. However, their evaluation is beyond the scope of this manuscript.

We also note, that incoherent exciton scattering processes such as Auger scattering [48, 49] and density-dependent exciton-phonon scattering [45, 47] are also fourth-order processes, which can be straightforwardly included in our theory by adding the respective interaction Hamiltonians in Eq. (1).

IV. EXCITONIC RABI OSCILLATIONS

We assume an undoped confined semiconductor and examine the two-dimensionally confined carrier dynamics via the total electron density N :

$$N = \frac{1}{\mathcal{A}} \sum_{\mathbf{k},\xi} \langle \hat{c}_{\mathbf{k}}^{\dagger\xi} \hat{c}_{\mathbf{k}}^{\xi} \rangle, \quad (45)$$

in units of one over area. Within an expansion in electron-hole operator pairs [23, 74], cf. Eq. (7), the total electron density N can also be expressed as:

$$N = \frac{1}{\mathcal{A}} \sum_{\mu,\mathbf{Q},\xi,\xi'} \left(|P_{\mu}^{\xi}|^2 \delta_{\mathbf{Q},\mathbf{0}} \delta_{\xi,\xi'} + N_{\mu,\mathbf{Q}}^{\xi,\xi'} \right), \quad (46)$$

where P_{μ}^{ξ} is the coherent excitonic transition from Eq. (13) and $N_{\mu,\mathbf{Q}}^{\xi,\xi'}$ is the incoherent excitonic occupation from Eq. (15). Note, that we truncated the expansion in electron-hole pairs, cf. Eq. (7) on a doublet level. A more complete treatment in fourth-order DCT would involve higher-order correlations up to quadruplets.

To study the exciton-density dynamics in Eq. (46), consider two cases, a monolayer MoSe₂ (strong Coulomb coupling) and a GaAs QW (less strong Coulomb coupling). Both systems are resonantly excited at $\hbar\omega_P = E_{1s}$ using a circularly polarized 2-ps pulse. We solve the excitonic equations of motion for the excitonic transitions P_{1s} and excitonic occupations $N_{1s,\mathbf{Q}}$. The equations of motion for the two-exciton continua $B_{+, \zeta, 1s}$ and exciton-two-exciton continua $Z_{+, \zeta, 1s, \mathbf{Q}}$ for $\xi = \xi' = K, \uparrow$ (monolayer MoSe₂) or $\xi = \xi' = \text{heavy-hole exciton}$ (GaAs QW) are eliminated via a Markov approximation, i.e., we assume an instantaneous build-up of exciton-exciton interaction and neglect memory effects [109], which is reasonable given the comparably long pulse duration. We take only $\mu = 1s$ excitonic transitions and occupations into account and neglect any intraexcitonic coherences $N_{\mu,\nu \neq \mu, \mathbf{Q}}$, but include $1s$, $2s$ and $3s$ excitonic states

in the calculation of the symmetric two-exciton continua $B_{+,\zeta}$ and symmetric exciton-two-exciton continua $Z_{+,\zeta}$. Due to the circular excitation, antisymmetric “-”-configurations, which host a bound biexciton/exciton-biexciton, are not induced.

For comparison with the excitonic theory, we also solve the well-established semiconductor Bloch equations in Hartree-Fock limit [11] to obtain the density of uncorrelated electrons in Eq. (45):

$$\begin{aligned} i\hbar\partial_t P_{\mathbf{k}} &= (E_{\mathbf{k}} - \hbar\omega_P - i\hbar\gamma_{\text{nrad}})P_{\mathbf{k}} - \sum_{\mathbf{q}} V_{\mathbf{q}-\mathbf{k}} P_{\mathbf{q}} \\ &- \hbar\Omega^{cv} (1 - 2n_{\mathbf{k}}) + 2 \sum_{\mathbf{q}} V_{\mathbf{q}-\mathbf{k}} (n_{\mathbf{k}} P_{\mathbf{q}} - n_{\mathbf{q}} P_{\mathbf{k}}), \quad (47) \\ i\hbar\partial_t n_{\mathbf{k}} &= \hbar\Omega^{vc} P_{\mathbf{k}} + \sum_{\mathbf{q}} V_{\mathbf{q}-\mathbf{k}} P_{\mathbf{q}}^* P_{\mathbf{k}} - \text{c.c.}, \end{aligned}$$

where $P_{\mathbf{k}} = \langle \hat{v}_{\mathbf{k}}^\dagger \hat{c}_{\mathbf{k}} \rangle$ is the interband transition, cf. also Eq. (13), and $n_{\mathbf{k}}^\xi$ are the electron occupations:

$$n_{\mathbf{k}}^\xi = \langle \hat{c}_{\mathbf{k}}^\dagger \hat{c}_{\mathbf{k}}^\xi \rangle. \quad (48)$$

All material parameters are listed in Tab. II. To ensure comparable conditions, we assume equal nonradiative dephasings γ_{nrad} for the MoSe₂ monolayer and GaAs QW and neglect any contributions due to reradiation [63]. In a MoSe₂ monolayer, a total (half) linewidth of 1 meV corresponds roughly to the radiatively-limited case, as the radiative (half) linewidth already approaches 1 meV, while in a GaAs QW, a total (half) linewidth of 1 meV is much larger than the radiative linewidth of approximately tens of μeV [62].

In the following, we dissect the corresponding interaction contributions to the exciton dynamics and compare the emerging dynamics of a MoSe₂ ML and a GaAs QW for circularly-polarized excitation (*GaAs QW vs. MoSe₂ monolayer*). Then, we identify the role of the coherent and (optically dark) incoherent exciton density (*Coherent vs. incoherent exciton density*) and examine the momentum distribution of optically dark excitons (*Momentum distribution of optically dark excitons*). At last, we compare circular and linear excitation in a MoSe₂ ML (*Circular vs. linear excitation*).

GaAs QW vs. MoSe₂ monolayer: In Fig. 7, we depict the dynamics of the electron density, cf. Eq. (45), by solving the semiconductor Bloch equations (SBEs) in Eq. (47) and the dynamics of the total excitonic density, cf. Eq. (46), as solutions of the full excitonic Bloch equations in Eqs. (21)–(44) within the limits discussed above at various pulse areas, defined in Eq. (26). The left column depicts simulations for a GaAs QW and the right column depicts the simulations for a h-BN-encapsulated MoSe₂ monolayer.

In Fig. 7(a,f), which shows the results from solving the SBEs, Eq. (47), Rabi flops are observed, whose period increases with increasing pulse area. In Fig. 7(a) (GaAs

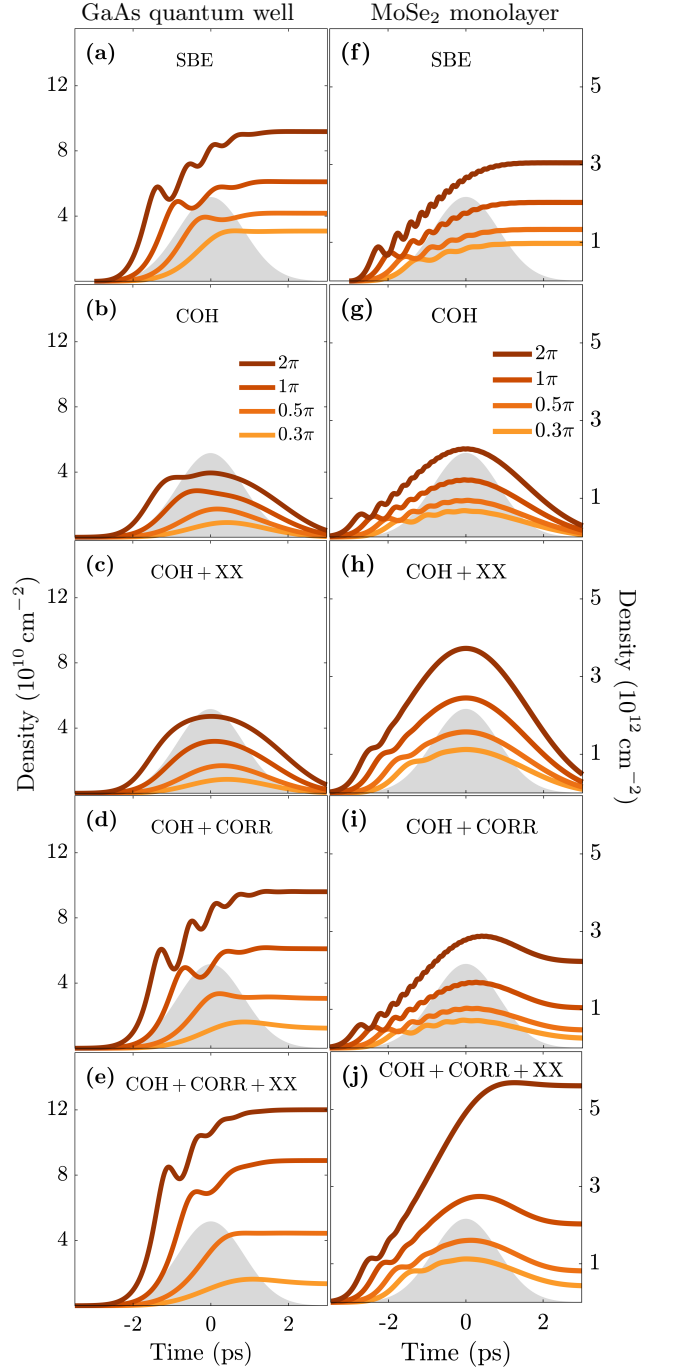


FIG. 7. Dynamics of the total electron density N from Eq. (45) as solution of the semiconductor Bloch equations (SBE) (a,f) compared to the total exciton density N from Eq. (46) as a solution of the excitonic Bloch equations in the coherent limit (COH) (b,g), with additional exciton-exciton scattering contributions (COH + XX) (c,h) and with additional correlated contributions (COH + CORR) (d,i) and with all contributions (COH + CORR + XX) (e,j) at various pulse areas Θ , cf. Eq. (26), for a 8-nm GaAs quantum well (left column) and for a MoSe₂ monolayer (right column). The grey-shaded area depicts the normalized pulse intensity.

TABLE II. Parameters used in the numerical calculations.

Intensity FWHM	2000 fs
Nonradiative (half) linewidth $\hbar\gamma_{\text{nrad}}$	1 meV
GaAs quantum well	
Real well width d	8 nm
Effective well width d_{eff}	$1.3d$ [110]
1s excitonic binding energy	−8.8 meV
$E_{1s} - \tilde{E}_{\text{gap}}$ (calculated)	
Static dielectric constant of GaAs	12.46 (5 K) [111]
Effective electron mass m_e	$0.0665m_0$ [112]
Effective heavy-hole mass m_h	$0.1106m_0$ [113]
h-BN-encapsulated MoSe ₂ monolayer	
Monolayer width d	0.6527 nm [114]
1s excitonic binding energy	−341 meV
$E_{1s} - \tilde{E}_{\text{gap}}$ (calculated)	
Biexcitonic binding energy	−19.3 meV
$E_{B,-,b} - 2E_{1s}$ (calculated)	
Static dielectric constant of bulk MoSe ₂	$\sqrt{8.2 \cdot 17.7}$ [115]
Effective electron mass m_e	$0.5m_0$ [116]
Effective hole mass m_h	$0.6m_0$ [116]
Plasmon energy of MoSe ₂ $\hbar\omega_{\text{pl}}$	22 eV [117]
TF screening parameter of MoSe ₂ α_{TF}	1.9 (adj. to CMR [118])
Static dielectric constant of bulk h-BN	4.8 [119]
Interlayer gap h	0.3 nm [120, 121]

QW), up to four Rabi flops can be observed at a pulse area of 2π , while Fig. 7(f) (MoSe₂ ML) shows a multitude of Rabi flops. As Rabi oscillations are enhanced due to the occurrence of Coulomb-induced internal fields, cf. last term in the first line in Eq. (47), and the Coulomb interaction in a MoSe₂ ML is much stronger compared to a GaAs QW due to the reduced screening, more Rabi flops occur in a MoSe₂ monolayer.

In Fig. 7(b,g), we depict the coherent (COH) limit of the excitonic Bloch equations, cf. Eq. (21) and Eq. (30), which corresponds to the excitonic description in Ref. [122], which does not include nonradiative dephasing. Here, the exciton density decays within 3 ps, as no long-lived incoherent occupations $N_{1s,\mathbf{Q}}$ are induced. In the GaAs QW, Fig. 7(b), one Rabi flop occurs at the largest pulse area, as the nonradiative dephasing $\hbar\gamma_{\text{nrad}}$ suppresses them. In a MoSe₂ monolayer, Fig. 7(g), Rabi flops occur in a similar number compared to the SBE-case in Fig. 7(f), since the stronger Coulomb-induced field renormalization counterbalances the nonradiative dephasing on short timescales.

In Fig. 7(c,h), we depict the coherent limit with exciton-exciton interaction corresponding to two-exciton continua (COH + XX), cf. Eq. (21), Eq. (30), Eq. (32) and Eq. (29), which corresponds to the model developed in Refs. [17, 18, 123]. In this limit, the two-exciton-induced dephasing, which corresponds to the coupling of excitonic transitions to two-exciton continua (excitation-induced dephasing) totally suppresses the (coherent) Rabi oscillations in the GaAs QW and greatly suppresses them in a MoSe₂ monolayer, but not

completely, as two Rabi flops of small amplitude still remain. The overall induced coherent exciton density is larger compared to Fig. 7(b,g), as the exciton-exciton interaction reduces the overall excitation-dependent blue shift due to bandgap reduction and phase-space filling in Eq. (30) (first line) enabling a more efficient optical excitation of electron-hole pairs. This is especially relevant in a MoSe₂ ML, as the enhanced Coulomb interaction causes a stronger exciton-exciton interaction and hence a stronger excitation-induced dephasing and -attenuation of the blue shift.

In Fig. 7(d,i), we turn off the exciton-exciton (XX) interaction in Eq. (32) and Eq. (29), but include the correlated contributions in Eq. (31), Eq. (34) and Eq. (35), i.e., we allow incoherent, optically dark excitonic occupations $N_{1s,\mathbf{Q}}$ to be induced via Coulomb-enhanced Pauli-blocking. Here, the exciton dynamics for the GaAs QW matches remarkably well the electron dynamics in the SBE in Fig. 7(a) with minor deviations at small pulse areas below 1π . In a MoSe₂ monolayer, Fig. 7(i), the Rabi flopping dynamics is very similar to the SBE-case in Fig. 7(f) until the pulse maximum is reached, from which on deviations occur, as the coherent excitation of incoherent and optically dark excitonic occupations is less effective compared to the GaAs QW.

In Fig. 7(e,j), we consider all contributions, i.e., we turn on again Eq. (32) as well as Eq. (29) and include Eq. (33), Eq. (43) and Eq. (44). Here, the Rabi-flopping dynamics for a GaAs QW are slightly suppressed compared to Fig. 7(d) due to the excitation-induced dephasing, which occurs via the two-exciton continuum $B_{+,\zeta}$, driven nonlinearly via $P_{1s}P_{1s}$, cf. Eq. (29), as well as via the exciton-two-exciton continuum $Z_{+,\zeta}$ driven by $P_{1s}N_{1s,\mathbf{Q}}$, cf. Eq. (33). For the MoSe₂ monolayer, almost all Rabi flops are suppressed, while only a few in the very beginning around −2 ps remain. In both cases, the GaAs QW and the MoSe₂ ML, the inclusion of exciton-exciton interaction enhances the overall optically injected exciton density with the most pronounced contribution in the MoSe₂ ML at the largest pulse areas. This amplification is caused by the red-shift contribution causing a more effective optical excitation of excitonic transitions, which, in turn, as the pulse area increases, leads to an enhanced coherent excitation of excitonic occupations in fourth order via $\hbar\Omega|P_{1s}|^2P_{1s}$, cf. Eq. (34).

All in all, our excitonic theory reproduces the key physics encoded in the semiconductor Bloch equations, which have been proven to reliably model Rabi flops in ultrafast experiments in the moderate Coulomb-interaction regime (GaAs QW) [6, 8, 12], while showing major deviations from the SBEs due to exciton-exciton interaction in the strong Coulomb-interaction regime (MoSe₂ ML). Here, in circular excitation, Rabi oscillations in the incoherent exciton density are effectively suppressed, while a few Rabi flops in the coherent exciton density can be eventually observed, if the linewidth does not exceed $2\hbar\gamma_{\text{nrad}} = 2 \text{ meV}$.

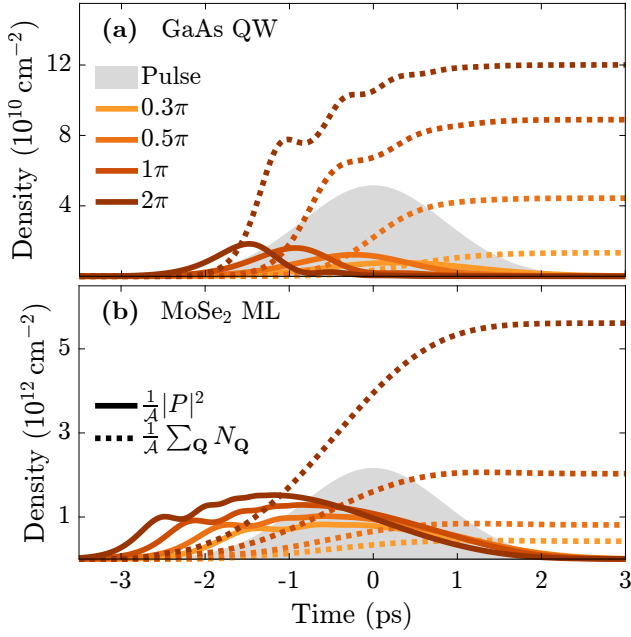


FIG. 8. Dynamics of the coherent exciton density $\frac{1}{\mathcal{A}}|P|^2$ (solid lines) and the incoherent exciton density $\frac{1}{\mathcal{A}}\sum_{\mathbf{Q}} N_{\mathbf{Q}}$ (dotted lines) for the full simulations of a GaAs quantum well and a h-BN-encapsulated MoSe₂ monolayer from Fig. 7(e,j).

Coherent vs. incoherent exciton density: To examine the different dynamical behavior of the GaAs QW and the MoSe₂ ML in more detail, we depict the individual coherent ($|P_{1s}|^2$, solid lines) and incoherent ($N_{1s,\mathbf{Q}}$, dotted lines) contributions in Fig. 8. It becomes clear, that the Rabi flopping in a GaAs QW occurs in the incoherent part of the total excitonic density $\frac{1}{\mathcal{A}}\sum_{\mathbf{Q}} N_{1s,\mathbf{Q}}$, while in a MoSe₂ monolayer, it occurs in the coherent part of the total exciton density $\frac{1}{\mathcal{A}}|P_{1s}|^2$. This is a consequence of the weaker Coulomb interaction in the GaAs QW, which does not significantly suppress fermionic Pauli-blocking effects in Eq. (31) (last line) leading to an efficient formation of incoherent, optically dark excitonic occupations $N_{1s,\mathbf{Q}}$ in fourth order, cf. Eq. (34) and Eq. (35). In a MoSe₂ ML, due to the stronger Coulomb interaction, fermionic Pauli-blocking effects are reduced, while, at the same time, the Coulomb-induced field renormalization, i.e., the excitonic Rabi energy, is enhanced. This leads to a regime, where Rabi oscillations preferably occur in the coherent exciton density and don't translate to the incoherent, optically dark exciton density.

Momentum distribution of optically dark excitons: In Fig. 9, we depict the momentum distribution of the coherently excited excitonic occupations $N_{1s,\mathbf{Q}}$ for a GaAs QW and a MoSe₂ ML. Similar to the fully bosonic theory in Ref. [33], our theory predicts a coherent excitation of excitonic occupations at center-of-mass momenta well outside the light cone (grey dotted vertical line). At

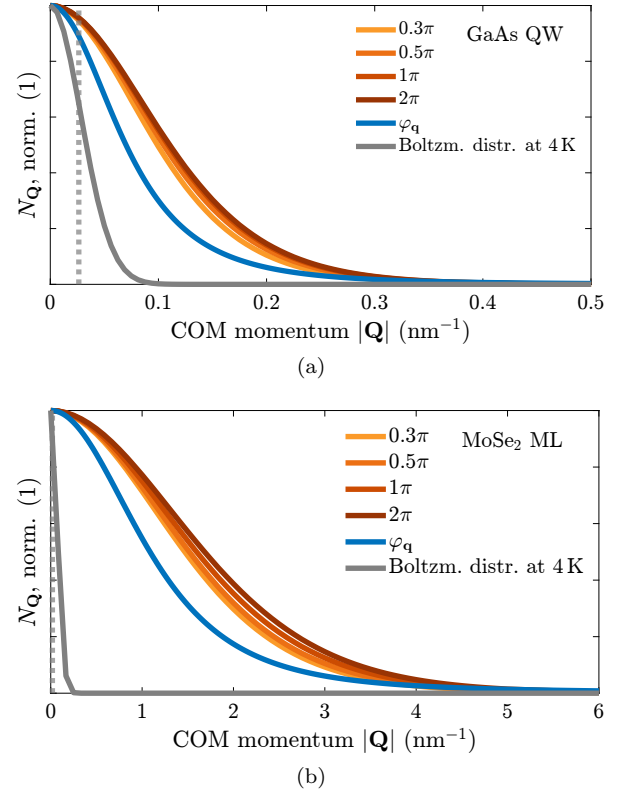


FIG. 9. Momentum distribution of the incoherent excitonic occupation $N_{1s,\mathbf{Q}}$ of a GaAs QW (a) and a h-BN-encapsulated MoSe₂ ML (b) after optical excitation at various pulse areas. Vertical dashed lines denote the light cone.

increasing pulse areas, the distribution becomes slightly broader. While the distribution in a GaAs QW is well localized in momentum space with an energy width of approximately 45 K, the distribution in a MoSe₂ ML is broad with an energy width of approximately 1500 K (note the different COM-momentum scale). This difference is a direct consequence of the different Coulomb interaction, cf. also the corresponding excitonic wave function $\varphi_{\mathbf{q}}$ (blue solid line): A stronger Coulomb interaction enhances the individual electron and hole collisions due to the fermionic substructure in the exciton gas, leading to broader distributed coherently excited excitonic occupations.

Circular vs. linear excitation: In Fig. 10, we depict the dynamics of the total exciton density at the K valley from Eq. (46), i.e., $\xi = \xi' = K, \uparrow$, for circular (a), cf. also Fig. 7(j), and linear (b) excitation. For the linear-excitation case, we include coherent transitions at the K and K' valleys $P_{1s}^K, P_{1s}^{K'}$ as well as intravalley incoherent occupations $N_{1s,\mathbf{Q}}^{K,K}, N_{1s,\mathbf{Q}}^{K',K'}$ and neglect any intervalley occupations $N_{1s,\mathbf{Q}}^{K,K'}/N_{1s,\mathbf{Q}}^{K',K}$. While in circular excitation, some Rabi flops of the coherent exciton density remain, cf. Fig. 8 and the discussion above, in linear excitation, even the Rabi flops in the coherent

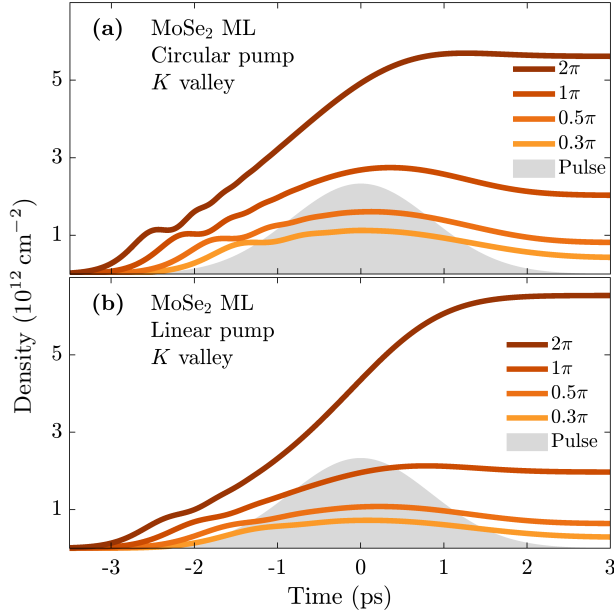


FIG. 10. Dynamics of the total exciton density $N = \frac{1}{\mathcal{A}}|P_{1s}^{K,\uparrow}|^2 + \frac{1}{\mathcal{A}}\sum_{\mathbf{Q}}N_{1s,\mathbf{Q}}^{K,\uparrow,K,\uparrow}$ at the K valley for circular excitation (a) and linear excitation (b) in a h-BN-encapsulated MoSe₂ monolayer.

exciton density are almost totally suppressed. The reason is the larger two-exciton/exciton-two-exciton phase space: In circular excitation, only symmetric (+) intravalley two-exciton continua $B_{+, \zeta}^{K,K,K,K}$ and exciton-two-exciton continua $Z_{+, \zeta, \mathbf{Q}}^{K,K,K,K}$ are induced. In linear excitation, the K valley and the K' valley are equally excited, so that additional symmetric (+) and antisymmetric (−) intervalley two-exciton continua $B_{\pm, \zeta}^{K,K',K',K}/B_{\pm, \zeta}^{K',K,K,K'}$ and exciton-two-exciton continua $Z_{\pm, \zeta, \mathbf{Q}}^{K',K',K,K,K',K'}/Z_{\pm, \zeta, \mathbf{Q}}^{K,K,K',K',K,K}$ are induced. These yield a dynamic coupling between the excitonic transitions at the K valley P_{1s}^K and at the K' valley $P_{1s}^{K'}$, hence further increasing the excitation-induced dephasing. Moreover, the formation of a bound (b) biexciton $B_{-, \zeta=b}^{K,K',K',K}/B_{-, \zeta=b}^{K',K,K,K'}$ and bound exciton-biexciton $Z_{-, \zeta=b, \mathbf{Q}}^{K',K',K,K,K',K'}/Z_{-, \zeta=b, \mathbf{Q}}^{K,K,K',K',K,K}$ becomes possible, further enhancing the excitation-induced dephasing. Hence, due to the overall larger number of Coulomb-interaction-induced exciton-exciton correlations and the resulting dynamic coupling of the excitonic transitions P between the K and K' valley, the excitation-induced

dephasing is larger in linear excitation compared to circular excitation causing a suppression of the Rabi oscillations in the coherent exciton density. This theoretical finding is consistent with recent experiments in a MoSe₂ monolayer, where a clear Rabi splitting due to an occupation grating, which is insensible to coherent excitation-induced dephasing, has been measured, but no Rabi oscillations could be observed [62].

V. CONCLUSION

In this work, we developed and discussed a theory for the ultrafast dynamics of Wannier excitons valid from the low-density regime up to an elevated-density regime below the Mott transition, which is unleashed on two distinct materials as proponents of different Coulomb-to-light-matter-interaction regimes: A GaAs quantum well with moderate Coulomb interaction and a MoSe₂ monolayer with strong Coulomb interaction compared to light-matter interaction. It has been found, that the excitonic approach reproduces the key physics described by the semiconductor Bloch equations well, which have been proven to reliably model Rabi flops in ultrafast experiments in the moderate Coulomb-interaction regime (GaAs QW) [6, 8, 12], while showing major deviations from the SBEs in the strong Coulomb-interaction regime (MoSe₂ ML) due to exciton-exciton interaction induced by Coulomb-correlated doublets and triplets, in line with recent experiments [62]. Here, in circular excitation, Rabi oscillations are considerably less strong and vanish almost completely in linear excitation. Our findings strongly indicate, that an excitonic approach has to be chosen to simulate the non-linear response of confined semiconductors, as long as the excitation conditions are below the Mott transition and correlated electron-hole pairs dominate. On the other hand, if the excitation conditions are above the Mott transition, where uncorrelated electrons and holes dominate, the expansion in correlated electron-hole pairs breaks down and the semiconductor Bloch equations need to be applied.

ACKNOWLEDGMENTS

Funded by the Deutsche Forschungsgemeinschaft (DFG, German Research Foundation) – Project No. 420760124 (H.M., A.K.); 556436549 (A.K.).

H.M. and A.K. thank Felix Schäfer, Markus Stein and Sangam Chatterjee (Justus-Liebig-Universität Gießen) for fruitful discussions and their measurements, which strongly motivated the theory developed here.

-
- [1] I. I. Rabi, *Phys. Rev.* **51**, 652 (1937).
 - [2] P. Knight and P. Milonni, *Phys. Rep.* **66**, 21 (1980).
 - [3] J. Danckwerts, K. J. Ahn, J. Förstner, and A. Knorr,

- Phys. Rev. B* **73**, 165318 (2006).
- [4] J. Förstner, C. Weber, J. Danckwerts, and A. Knorr, *Phys. Rev. Lett.* **91**, 127401 (2003).

- [5] L. Dominici, D. Colas, S. Donati, J. P. Restrepo Cuartas, M. De Giorgi, D. Ballarini, G. Guirales, J. C. López Carreño, A. Bramati, G. Gigli, E. del Valle, F. P. Laussy, and D. Sanvitto, *Phys. Rev. Lett.* **113**, 226401 (2014).
- [6] A. Schülzgen, R. Binder, M. E. Donovan, M. Lindberg, K. Wundke, H. M. Gibbs, G. Khitrova, and N. Peyghambarian, *Phys. Rev. Lett.* **82**, 2346 (1999).
- [7] H. Giessen, A. Knorr, S. Haas, S. Koch, S. Linden, J. Kuhl, M. Hetterich, M. Grün, and C. Klingshirn, *Phys. Rev. Lett.* **81**, 4260 (1998).
- [8] S. T. Cundiff, A. Knorr, J. Feldmann, S. W. Koch, E. O. Göbel, and H. Nickel, *Phys. Rev. Lett.* **73**, 1178 (1994).
- [9] T. Kuhn and F. Rossi, *Phys. Rev. Lett.* **69**, 977 (1992).
- [10] R. Binder, S. W. Koch, M. Lindberg, N. Peyghambarian, and W. Schäfer, *Phys. Rev. Lett.* **65**, 899 (1990).
- [11] M. Lindberg and S. W. Koch, *Phys. Rev. B* **38**, 3342 (1988).
- [12] R. H. Binder, M. Lindberg, A. Schuelzgen, M. E. Donovan, K. Wundke, H. M. Gibbs, G. Khitrova, and N. Peyghambarian, in *Physics and Simulation of Optoelectronic Devices VII*, Vol. 3625, edited by P. Blood, A. Ishibashi, and M. Osinski, International Society for Optics and Photonics (SPIE, 1999) pp. 80 – 87.
- [13] A. Steinhoff, F. Jahnke, and M. Florian, *Phys. Rev. B* **112**, 115415 (2025).
- [14] R. Takayama, N. H. Kwong, I. Rumyantsev, M. Kuwata-Gonokami, and R. Binder, *Eur. Phys. J. B* **25**, 445 (2002).
- [15] M. Buck, L. Wischmeier, S. Schumacher, G. Czycholl, F. Jahnke, T. Voss, I. Rückmann, and J. Gutowski, *Eur. Phys. J. B* **42**, 175 (2004).
- [16] A. Steinhoff, M. Florian, A. Singh, K. Tran, M. Kolarczik, S. Helmrich, A. W. Achtstein, U. Woggon, N. Owschimikow, F. Jahnke, and X. Li, *Nat. Phys.* **14**, 1199 (2018).
- [17] F. Katsch, M. Selig, and A. Knorr, *2D Mater.* **7**, 015021 (2019).
- [18] F. Katsch, M. Selig, and A. Knorr, *Phys. Rev. Lett.* **124**, 257402 (2020).
- [19] J. Tang and C.-Z. Ning, *Phys. Rev. B* **111**, L161409 (2025).
- [20] M. M. Dignam, F. Sy, A. M. Parks, and D. Wang, *AIP Conf. Proc.* **1590**, 20 (2014).
- [21] A. M. Parks, M. M. Dignam, and D. Wang, *Phys. Rev. B* **87**, 205306 (2013).
- [22] V. M. Axt, G. Bartels, and A. Stahl, *Phys. Rev. Lett.* **76**, 2543 (1996).
- [23] F. Katsch, M. Selig, A. Carmele, and A. Knorr, *Phys. Status Solidi (B)* **255**, 1800185 (2018).
- [24] V. M. Axt and A. Stahl, *Z. Phys. B: Condens. Matter* **93**, 195 (1994).
- [25] K. Victor, V. M. Axt, and A. Stahl, *Phys. Rev. B* **51**, 14164 (1995).
- [26] T. Usui, *Prog. Theor. Phys.* **23**, 787 (1960).
- [27] G. Rochat, C. Ciuti, V. Savona, C. Piermarocchi, A. Quattropani, and P. Schwendimann, *Phys. Rev. B* **61**, 13856 (2000).
- [28] D. Wang and M. M. Dignam, *Phys. Rev. B* **79**, 165320 (2009).
- [29] D. Wang, M. Hawton, and M. M. Dignam, *Phys. Rev. B* **76**, 115311 (2007).
- [30] V. M. Axt, S. R. Bolton, U. Neukirch, L. J. Sham, and D. S. Chemla, *Phys. Rev. B* **63**, 115303 (2001).
- [31] T. Östreich and A. Knorr, *Phys. Rev. B* **50**, 5717 (1994).
- [32] V. M. Axt, B. Haase, and U. Neukirch, *Phys. Rev. Lett.* **86**, 4620 (2001).
- [33] Z. S. Yang, N.-H. Kwong, R. Takayama, and R. Binder, *EPL* **69**, 417 (2004).
- [34] N. Takemura, M. D. Anderson, S. Trebaol, S. Biswas, D. Y. Oberli, M. T. Portella-Oberli, and B. Deveaud, *Phys. Rev. B* **92**, 235305 (2015).
- [35] N. Takemura, M. D. Anderson, S. Biswas, M. Navadeh-Toupchi, D. Y. Oberli, M. T. Portella-Oberli, and B. Deveaud, *Phys. Rev. B* **94**, 195301 (2016).
- [36] M. Combescot, M. A. Dupertuis, and O. Betbeder-Matibet, *EPL* **79**, 17001 (2007).
- [37] H. Rose, S. Schumacher, and T. Meier, *arXiv preprint arXiv:2506.22220* (2025), 10.48550/arXiv.2506.22220.
- [38] E. V. Denning, A. Knorr, F. Katsch, and M. Richter, *Phys. Rev. Lett.* **129**, 097401 (2022).
- [39] E. V. Denning, A. Knorr, F. Katsch, and M. Richter, *Phys. Rev. B* **106**, 195307 (2022).
- [40] G. H. Wannier, *Phys. Rev.* **52**, 191 (1937).
- [41] T. Deckert, H. Mittenzwey, O. Dogadov, M. Bertolotti, G. Cerullo, D. Brida, A. Knorr, and S. Dal Conte, *Phys. Rev. Lett.* **135**, 066902 (2025).
- [42] A. Thränhardt, S. Kuckenburg, A. Knorr, T. Meier, and S. W. Koch, *Phys. Rev. B* **62**, 2706 (2000).
- [43] M. Selig, G. Berghäuser, M. Richter, R. Bratschitsch, A. Knorr, and E. Malic, *2D Mater.* **5**, 035017 (2018).
- [44] S. Brem, A. Ekman, D. Christiansen, F. Katsch, M. Selig, C. Robert, X. Marie, B. Urbaszek, A. Knorr, and E. Malic, *Nano Lett.* **20**, 2849 (2020).
- [45] M. Katzer, M. Selig, L. Sigl, M. Troue, J. Figueiredo, J. Kiemle, F. Sigger, U. Wurstbauer, A. W. Holleitner, and A. Knorr, *Phys. Rev. B* **108**, L121102 (2023).
- [46] V. R. Policht, H. Mittenzwey, O. Dogadov, M. Katzer, A. Villa, Q. Li, B. Kaiser, A. M. Ross, F. Scognella, X. Zhu, A. Knorr, M. Selig, G. Cerullo, and S. Dal Conte, *Nat. Commun.* **14**, 7273 (2023).
- [47] M. Katzer, M. Selig, and A. Knorr, *Phys. Rev. B* **109**, 155110 (2024).
- [48] D. Erkensten, S. Brem, K. Wagner, R. Gillen, R. Perea-Causin, J. D. Ziegler, T. Taniguchi, K. Watanabe, J. Maultzsch, A. Chernikov, and E. Malic, *Phys. Rev. B* **104**, L241406 (2021).
- [49] A. Steinhoff, F. Jahnke, and M. Florian, *Phys. Rev. B* **104**, 155416 (2021).
- [50] H. Haug and S. W. Koch, *Quantum Theory of the Optical and Electronic Properties of Semiconductors*, 5th ed. (World Scientific, 2009).
- [51] F. Jahnke, M. Kira, and S. W. Koch, *Z. Phys. B: Condens. Matter* **104**, 559 (1997).
- [52] D. Y. Qiu, T. Cao, and S. G. Louie, *Phys. Rev. Lett.* **115**, 176801 (2015).
- [53] T. Yu and M. W. Wu, *Phys. Rev. B* **89**, 205303 (2014).
- [54] M. Combescot, T. Amand, and S.-Y. Shiao, *Phys. Rev. B* **107**, 115206 (2023).
- [55] N.-H. Kwong, J. R. Schaibley, and R. Binder, *Phys. Rev. B* **104**, 245434 (2021).
- [56] M. Selig, F. Katsch, R. Schmidt, S. Michaelis de Vasconcellos, R. Bratschitsch, E. Malic, and A. Knorr, *Phys. Rev. Res.* **1**, 022007 (2019).
- [57] M. Selig, F. Katsch, S. Brem, G. F. Mkrtchian, E. Malic, and A. Knorr, *Phys. Rev. Res.* **2**, 023322 (2020).
- [58] A. Torche and G. Bester, *Commun. Phys.* **4**, 67 (2021).
- [59] O. Dogadov, H. Mittenzwey, M. Bertolotti, N. Olsen,

- T. Deckert, C. Trovatiello, X. Zhu, D. Brida, G. Cerullo, A. Knorr, and S. Dal Conte, [arXiv preprint arXiv:2507.16665 \(2025\)](#), [10.48550/arXiv.2507.16665](#).
- [60] G. Berghäuser, I. Bernal-Villamil, R. Schmidt, R. Schneider, I. Niehues, P. Erhart, S. Michaelis de Vasconcellos, R. Bratschitsch, A. Knorr, and E. Malic, *Nat. Commun.* **9**, 971 (2018).
- [61] I. Bernal-Villamil, G. Berghäuser, M. Selig, I. Niehues, R. Schmidt, R. Schneider, P. Tonndorf, P. Erhart, S. M. de Vasconcellos, R. Bratschitsch, A. Knorr, and E. Malic, *2D Mater.* **5**, 025011 (2018).
- [62] F. Schäfer, H. Mittenzwey, M. Stein, O. Voigt, L. Greten, D. Anders, I. Müller, F. Dobener, M. Cuccu, C. Fuchs, K. Watanabe, T. Taniguchi, A. Chernikov, K. Volz, A. Knorr, and S. Chatterjee, *Nat. Commun.* **16**, 8109 (2025).
- [63] A. Knorr, S. Hughes, T. Stroucken, and S. W. Koch, *Chem. Phys.* **210**, 27 (1996), confined Excitations in Molecular and Semiconductor Nanostructures.
- [64] C. Aversa and J. E. Sipe, *Phys. Rev. B* **52**, 14636 (1995).
- [65] B. Gu, N. H. Kwong, and R. Binder, *Phys. Rev. B* **87**, 125301 (2013).
- [66] U. Huttner, M. Kira, and S. W. Koch, *Laser Photonics Rev.* **11**, 1700049 (2017).
- [67] S. A. Oliaei Motlagh, V. Apalkov, and M. I. Stockman, *Phys. Rev. B* **103**, 155416 (2021).
- [68] W. D. Rice, J. Kono, S. Zybelle, S. Winnerl, J. Bhattacharyya, H. Schneider, M. Helm, B. Ewers, A. Chernikov, M. Koch, S. Chatterjee, G. Khitrova, H. M. Gibbs, L. Schneebeli, B. Breddermann, M. Kira, and S. W. Koch, *Phys. Rev. Lett.* **110**, 137404 (2013).
- [69] T. Stroucken, J. Neuhaus, and S. W. Koch, *Phys. Rev. B* **104**, 075438 (2021).
- [70] T. Meier, H. Kolbe, A. Thränhardt, G. Weiser, P. Thomas, and S. Koch, *Phys. E: Low-Dimens. Syst. Nanostructures* **7**, 267 (2000).
- [71] T. Meier, F. Rossi, P. Thomas, and S. Koch, *Phys. Rev. Lett.* **75**, 2558 (1995).
- [72] F. Langer, C. P. Schmid, S. Schlauderer, M. Gmitra, J. Fabian, P. Nagler, C. Schüller, T. Korn, P. G. Hawkins, J. T. Steiner, U. Huttner, S. W. Koch, M. Kira, and R. Huber, *Nature* **557**, 76 (2018).
- [73] M. Borsch, M. Meierhofer, R. Huber, and M. Kira, *Nat. Rev. Mater.* **8**, 668 (2023).
- [74] A. L. Ivanov and H. Haug, *Phys. Rev. B* **48**, 1490 (1993).
- [75] J. Fricke, *Ann. Phys.* **252**, 479 (1996).
- [76] M. Kira and S. W. Koch, *Prog. Quantum Electron.* **30**, 155 (2006).
- [77] W. Hoyer, M. Kira, and S. Koch, *Phys. Status Solidi (B)* **234**, 195 (2002).
- [78] M. Combescot, O. Betbeder-Matibet, and R. Combescot, *Phys. Rev. B* **75**, 174305 (2007).
- [79] S. A. Moskalenko, *Opt. Spektrosk.* **5**, 147 (1958).
- [80] M. A. Lampert, *Phys. Rev. Lett.* **1**, 450 (1958).
- [81] L. N. Ivanov, Y. E. Lozovik, and D. R. Musin, *Journal of Physics C: Solid State Physics* **11**, 2527 (1978).
- [82] S. Schumacher, G. Czycholl, and F. Jahnke, *Phys. Rev. B* **73**, 035318 (2006).
- [83] W. Schäfer, D. S. Kim, J. Shah, T. C. Damen, J. E. Cunningham, K. W. Goossen, L. N. Pfeiffer, and K. Köhler, *Phys. Rev. B* **53**, 16429 (1996).
- [84] T. Meier, C. Sieh, E. Finger, W. Stolz, W. W. Rühle, P. Thomas, S. W. Koch, and A. D. Wieck, *Phys. Status Solidi (B)* **238**, 537 (2003).
- [85] G. Bartels, V. M. Axt, K. Victor, A. Stahl, P. Leisching, and K. Köhler, *Phys. Rev. B* **51**, 11217 (1995).
- [86] L. Bányai, Q. T. Vu, B. Mieck, and H. Haug, *Phys. Rev. Lett.* **81**, 882 (1998).
- [87] C. Ciuti, C. Piermarocchi, V. Savona, P. E. Selmann, P. Schwendimann, and A. Quattropani, *Phys. Rev. Lett.* **84**, 1752 (2000).
- [88] M. Selig, G. Berghäuser, A. Raja, P. Nagler, C. Schüller, T. F. Heinz, T. Korn, A. Chernikov, E. Malic, and A. Knorr, *Nat. Commun.* **7**, 13279 (2016).
- [89] F. Lengers, T. Kuhn, and D. E. Reiter, *Phys. Rev. B* **101**, 155304 (2020).
- [90] N. Ma and D. Jena, *Phys. Rev. X* **4**, 011043 (2014).
- [91] D. Jena and A. Konar, *Phys. Rev. Lett.* **98**, 136805 (2007).
- [92] S. Glutsch and F. Bechstedt, *Phys. Rev. B* **50**, 7733 (1994).
- [93] A. Thränhardt, C. Ell, S. Mosor, G. Rupper, G. Khitrova, H. M. Gibbs, and S. W. Koch, *Phys. Rev. B* **68**, 035316 (2003).
- [94] A. Raja, L. Waldecker, J. Zipfel, Y. Cho, S. Brem, J. D. Ziegler, M. Kulig, T. Taniguchi, K. Watanabe, E. Malic, T. F. Heinz, T. C. Berkelbach, and A. Chernikov, *Nat. Nanotechnol.* **14**, 832 (2019).
- [95] S. Pfalz, R. Winkler, T. Nowitzki, D. Reuter, A. D. Wieck, D. Hägele, and M. Oestreich, *Phys. Rev. B* **71**, 165305 (2005).
- [96] G. F. Mkrtchian, A. Knorr, and M. Selig, *Phys. Rev. B* **100**, 125401 (2019).
- [97] O. Hess and T. Kuhn, *Phys. Rev. A* **54**, 3347 (1996).
- [98] O. Hess and T. Kuhn, *Phys. Rev. A* **54**, 3360 (1996).
- [99] K. Wagner, J. Zipfel, R. Rosati, E. Wietek, J. D. Ziegler, S. Brem, R. Perea-Causín, T. Taniguchi, K. Watanabe, M. M. Glazov, E. Malic, and A. Chernikov, *Phys. Rev. Lett.* **127**, 076801 (2021).
- [100] R. Rosati, K. Wagner, S. Brem, R. Perea-Causín, J. D. Ziegler, J. Zipfel, T. Taniguchi, K. Watanabe, A. Chernikov, and E. Malic, *Nanoscale* **13**, 19966 (2021).
- [101] J. Zipfel, M. Kulig, R. Perea-Causín, S. Brem, J. D. Ziegler, R. Rosati, T. Taniguchi, K. Watanabe, M. M. Glazov, E. Malic, and A. Chernikov, *Phys. Rev. B* **101**, 115430 (2020).
- [102] H. Zhao, B. Dal Don, S. Moehl, H. Kalt, K. Ohkawa, and D. Hommel, *Phys. Rev. B* **67**, 035306 (2003).
- [103] V. M. Axt, K. Victor, and A. Stahl, *Phys. Rev. B* **53**, 7244 (1996).
- [104] M. Kira, W. Hoyer, T. Stroucken, and S. W. Koch, *Phys. Rev. Lett.* **87**, 176401 (2001).
- [105] M. Kira, W. Hoyer, and S. W. Koch, *Phys. Status Solidi (B)* **238**, 443 (2003).
- [106] W. Langbein and J. M. Hvam, *Phys. Rev. B* **61**, 1692 (2000).
- [107] Z. Ye, L. Waldecker, E. Y. Ma, D. Rhodes, A. Antony, B. Kim, X.-X. Zhang, M. Deng, Y. Jiang, Z. Lu, D. Smirnov, K. Watanabe, T. Taniguchi, J. Hone, and T. F. Heinz, *Nat. Commun.* **9**, 3718 (2018).
- [108] Y. Hayamizu, M. Yoshita, Y. Takahashi, H. Akiyama, C. Z. Ning, L. N. Pfeiffer, and K. W. West, *Phys. Rev. Lett.* **99**, 167403 (2007).
- [109] V. M. Axt, T. Kuhn, B. Haase, U. Neukirch, and J. Gutowski, *Phys. Rev. Lett.* **93**, 127402 (2004).
- [110] A. Liu, *Phys. Rev. B* **50**, 8569 (1994).
- [111] W. J. Moore and R. T. Holm, *J. Appl. Phys.* **80**, 6939

- (1996).
- [112] R. Binder, I. Galbraith, and S. W. Koch, *Phys. Rev. B* **44**, 3031 (1991).
 - [113] M. N. Bataev, M. A. Chukeev, M. M. Sharipova, P. A. Belov, P. S. Grigoryev, E. S. Khramtsov, I. V. Ignatiev, S. A. Eliseev, V. A. Lovtcius, and Y. P. Efimov, *Phys. Rev. B* **106**, 085407 (2022).
 - [114] I. Kylänpää and H.-P. Komsa, *Phys. Rev. B* **92**, 205418 (2015).
 - [115] A. Laturia, M. L. Van de Put, and W. G. Vandenberghe, *npj 2D Mater. Appl.* **2**, 6 (2018).
 - [116] A. Kormányos, G. Burkard, M. Gmitra, J. Fabian, V. Zólyomi, N. D. Drummond, and V. Fal'ko, *2D Mater.* **2**, 022001 (2015).
 - [117] A. Kumar and P. K. Ahluwalia, *Phys. B: Condens. Matter* **407**, 4627 (2012).
 - [118] K. Andersen, S. Latini, and K. S. Thygesen, *Nano Lett.* **15**, 4616 (2015).
 - [119] S. Latini, T. Olsen, and K. S. Thygesen, *Phys. Rev. B* **92**, 245123 (2015).
 - [120] M. Florian, M. Hartmann, A. Steinhoff, J. Klein, A. W. Holleitner, J. J. Finley, T. O. Wehling, M. Kaniber, and C. Gies, *Nano Lett.* **18**, 2725 (2018).
 - [121] M. Drüppel, T. Deilmann, P. Krüger, and M. Rohlfing, *Nat. Commun.* **8**, 2117 (2017).
 - [122] A. Knorr, T. Östreich, K. Schönhammer, R. Binder, and S. W. Koch, *Phys. Rev. B* **49**, 14024 (1994).
 - [123] F. Katsch and A. Knorr, *Phys. Rev. X* **10**, 041039 (2020).